Université de Montréal

Analyse de spectres FUSE d'étoiles naines blanches riches en hélium et mesure de leur abondance en carbone

par

Nicolas Petitclerc

Département de physique

Faculté des arts et des sciences

Mémoire présenté à la Faculté des études supérieures

en vue de l'obtention du grade de

Maître ès sciences (M.Sc.)

en physique

Mai, 2004

Université de Montréal

Faculté des études supérieures

Ce mémoire intitulé:

Analyse de spectres FUSE d'étoiles naines blanches riches en hélium et mesure de leur abondance en carbone

présenté par:

Nicolas Petitclerc

a été évalué par un jury composé des personnes suivantes:

Gilles Fontaine,	président-rapporteur
François Wesemael,	directeur de recherche
Paul Charbonneau,	membre du jury

Mémoire accepté le: _____

Sommaire

Les étoiles naines blanches de type spectral DB sont des objets dont la photosphère est composée presque exclusivement d'hélium neutre. Nous présentons ici une analyse détaillée des premiers spectres dans l'ultraviolet lointain disponibles pour ce type d'objet. Les spectres à haute résolution des trois objets GD 190, BPM 17088 et EC 20058-5234 ont été obtenus à partir du télescope spatial FUSE. Des transitions associées à plusieurs états d'ionisation du carbone sont observées dans le spectre des trois étoiles. Afin de déterminer l'abondance de carbone de façon convaincante, nous avons, en premier lieu, redéterminé à l'aide de données d'archives, les paramètres atmosphériques de base (température effective, abondance d'hydrogène et gravité de surface) de ces objets. Dans ce but, nous avons mis la main sur des spectres dans le domaine visible, afin de modéliser les larges raies d'hélium qu'ils contiennent. Nous avons également déterminé la température de ces objets de façon indépendante en modélisant leur distribution d'énergie. Une bonne cohérence interne émerge de nos analyses, et permet de contraindre l'abondance de carbone dans nos trois cibles à l'intervalle $-6.2 < log(C/He) < -5.5$.

La présence de carbone en abondance non négligeable dans les atmosphères d'étoiles de type DB constitue un véritable défi pour la théorie de l'évolution spectrale de ces objets. Les processus physiques invoqués jusqu'à présent n'arrivent pas en effet à rendre compte de la présence de cet élément aux températures effectives caractéristiques des étoiles de type DB. Nous suggérons que la présence d'un faible vent stellaire dans les couches externes de l'étoile pourrait ralentir la sédimentation du carbone qui serait le

résidu des phases évolutives précédentes.

Mots clefs:

GD 190 — BPM 170888 — EC 20058-5234 — Spectrophotométrie — Naines blanches — DB — Carbone — FUSE — Vent

Abstract

We present a comprehensive analysis of the far-ultraviolet spectra of three DB white dwarfs secured with the FUSE observatory. Transitions associated with various carbon ions are detected in all three objects. Atmospheric parameters are first redetermined on the basis of an analysis of archival data available, and the abundance of carbon, together with upper limits on the abundances of other heavy elements, are determined from the FUSE spectra. The log (C/He) ratios cover the range between −5.5 and −6.0. The presence of carbon, now detected in five DB stars with effective temperatures above 20,000 K, cannot be accounted for easily by physical processes currently thought to operate in the envelopes of DB stars. We suggest that a weak stellar wind threading the outer stellar layers of DB stars might sufficiently disrupt the settling of carbon leftover from the PG1159 phase to account for the carbon seen in the ultraviolet spectra of these objects.

Key words:

GD 190 — BPM 170888 — EC 20058-5234 — Spectrophotometry — White dwarf — DB — Carbon — FUSE — Wind

Table des matières

Liste des figures

Liste des tableaux

Chapitre 1

Introduction au mémoire

Les étoiles, depuis toujours un objet de fascination et d'émerveillement, n'en sont pas moins mortelles. La plupart d'entre elles, soit celles caractérisées par une masse inférieure à $\sim$8 $M_{\odot}$, termineront leur vie sous la forme d'une naine blanche après avoir brûlé suffisamment d'hydrogène et d'hélium pour quitter la séquence principale et la branche horizontale, respectivement. Ces cadavres stellaires sont constitués typiquement d'un noyau isotherme de matière dégénérée, qui contient plus de 99% de la masse de l'étoile, entouré d'une mince couche opaque isolante de matière non dégénérée. L'opacité de l'enveloppe restreint les observations photométriques et spectroscopiques aux couches les plus externes de l'étoile. Ces régions sont néanmoins très importantes puisque, en raison de leur grande opacité à la radiation, elles régularisent la perte d'énergie et contrôlent par conséquent l'évolution de l'étoile. L'évolution des étoiles naines blanches revient donc à un long refroidissement, qui est cependant accompagné de nombreux changements dans la composition chimique de la photosphère. Ainsi, la composition atmosphérique de ces objets peut servir de piste pour retracer leur mode de vie et leur évolution jusqu'à la mort.

Les étoiles naines blanches existent dans un large éventail de températures et de compositions chimiques de surface. La nomenclature établie afin de les classifier est

résumée par Wesemael et al. (1993). On regroupe ces objets sous deux types principaux. Les DA représentent environ 80% de la population recensée. Elles sont caractérisées par la présence de raies de Balmer très larges dans leur spectre visible, et leur photosphère est constituée presque exclusivement d'hydrogène. En fait la photosphère des naines blanches est généralement d'une pureté chimique impressionnante. Cette particularité s'explique par le champ gravitationnel intense (log g$\sim$ 8) présent à la surface de ces objets compacts. Ce dernier est à l'origine d'un processus de sédimentation très efficace, qui ne maintient que les élements les plus légers en surface (Schatzman 1958).

Entre 13 000 K et 30 000 K, les DB représentent l'autre type statistiquement important. Ces étoiles sont caractérisées par leur spectre visible riche en raies de He I; leur photosphère est en fait dominée par l'hélium, l'élément le plus léger après l'hydrogène. Les DB, étant moins nombreuses et moins lumineuses, sont des objets moins bien connus et l'on se pose encore certaines questions fondamentales à leur sujet. Par exemple, pourquoi l'atmosphère de ces objets est-elle dépourvue d'hydrogène ? Ou encore, c'est la question mise en lumière ici, d'où proviennent les traces de carbone observées dans l'atmosphère des étoiles DB ?

Il existe évidemment plusieurs autres processus physiques qui peuvent compétitionner avec le tri gravitationnel afin d'expliquer les abondances chimiques présentes dans l'atmosphère des naines blanches. Un de ceux-ci est la convection de surface, qui apparaît dans les régime de température associés à la recombinaison de l'hélium (moins de 60 000 K) pour les DB ou de l'hydrogène (moins de 15 000 K) pour les DA (Fontaine & Wesemael 1987). Pour les étoiles chaudes, au-delà de $\sim$20 000k pour les DA et de $\sim$30 000 K pour les non-DA, l'accélération radiative est significative et permet la lévitation sélective d'éléments lourds. Cependant l'abondance de ces éléments observée dans les étoiles DA n'est pas très cohérente avec les prédictions de la théorie de la lévitation radiative. On croit que la présence d'un faible vent stellaire pourrait être la cause de ce désaccord (Fontaine & Wesemael 1991). On considère également que l'accrétion de

matière provenant du milieu interstellaire peut contribuer de façon significative à enrichir en éléments lourds l'atmosphère des naines blanches les plus froides. Cependant, même en tenant compte de tout ces processus physiques, il semblait impossible, jusqu'à récemment, d'expliquer la présence de traces de carbone dans l'atmosphère des naines blanches de type DB. Même l'idée plus récente (Dehner & Kawaler 1995; Brassard & Fontaine 2002, 2003) d'une connexion évolutive des étoiles PG 1159 aux naines blanches DO et DB, n'a pu résoudre cette énigme. On suggère, dans ces articles, que la séparation de l'hélium du carbone et de l'oxygène n'est peut-être pas complétée au moment où une étoile devient DB ($T_{\rm eff} < 30,000\,{\rm K}$), contrairement à ce qui était envisagé auparavant. Malheureusement, les abondances de carbone résiduel prédites sont considérablement en deçà des valeurs observées.

D'un point de vue observationnel, le télescope spatial FUSE (Far Ultraviolet Spectroscopic Explorer) nous permet l'observation dans une région spectrale particulièrement propice à l'étude des abondances en éléments lourds des étoiles de type DB. L'utraviolet lointain regorge en effet de fortes transitions liant le niveau fondamental de nombreux éléments.

Le but de ce projet est de mesurer, ou du moins contraindre, l'abondance photosphérique d'éléments lourds dans les trois naines blanches de type DB observées jusqu'à présent à l'aide du satellite FUSE: GD 190, BPM 17088 et EC 20058-5234. Les abondances que nous déterminons dépendent évidemment des autres paramètres atmosphériques, tels que la température effective, l'abondance d'hydrogène et la gravité de surface. Nous avons donc utilisé les données disponibles dans plusieurs archives astronomiques afin de contraindre, au préalable, ces paramètres. Nous avons ainsi utilisé des spectres d'archive dans le domaine visible, afin de modéliser les larges raies d'hélium neutre, de la même façon que Beauchamp et al. (1999). Cette procédure permet une détermination des trois paramètres atmosphériques de base, $T_{\rm eff}$, $\log g$ et le rapport H/He. Nous avons également redéterminé de façon indépendante la température de ces

objets en en modélisant la distribution d'énergie, les données spectrophotométriques disponibles s'étendant du proche infrarouge jusqu'à l'ultraviolet lointain. Une fois ce travail accompli, nous avons déterminé l'abondance de carbone dans nos trois cibles.

L'échantillon d'étoiles DB pour lesquelles des mesures du rapport C/He existent contient maintenant cinq objets. Afin de dresser un portrait complet des patrons d'abondance de carbone dans ce type d'étoiles, nous avons également réévalué les limites supérieures obtenues dans plus d'une douzaine de ces étoiles par Wegner & Nelan (1987). Cette étape apparaît nécessaire, étant donné que les spectres IUE à faible dispersion archivés sur lesquels l'étude se basait ont tous été, depuis, recalibrés.

Finalement, nous rediscutons des modèles qui tentent d'expliquer la présence d'un élément lourd comme le carbone dans les photosphères à haute gravité des étoiles naines blanches de type DB. Nous suggérons qu'une légère modification au modèle d'évolution des étoiles DB, l'inclusion d'un vent stellaire associé à un modeste taux de perte de masse ($\dot{M} \sim 10^{-13}\, M_{\odot}\, \mathrm{yr}^{-1}$), pourrait rendre compte des observations.

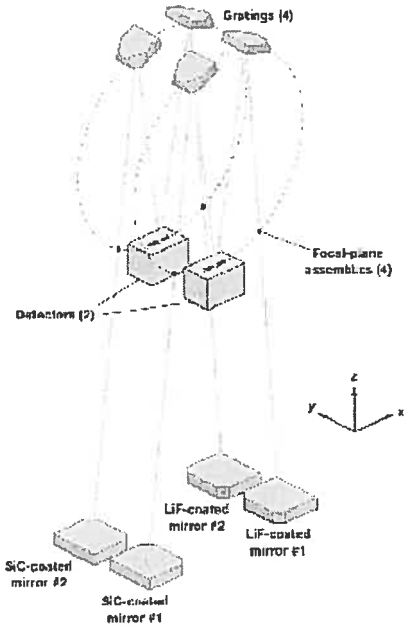

FIGURE 1.1 – Schéma du système optique du satellite FUSE.

1.1 FUSE

Le satellite FUSE fait environ 5.5 m de long et a une masse de ~1300 kg. Lancé le 24 juin 1999, il circule depuis sur une orbite quasi circulaire relativement basse de 768 km (Moos et al. 2000). Il permet d'observer des objets peu lumineux dans la région spectrale de l'ultraviolet lointain (905-1187 Å) avec une résolution spectrale ($R \equiv \lambda/\Delta\lambda$) entre 12 000 et 30 000. Il y a trois choix de diaphragme, le plus commun (LWRS) est de 30" x 30" d'angle sur le ciel, mais des ouvertures de 4" x 20" et de 1".25 x 20" sont également possibles.

La spectroscopie à haute résolution dans l'ultraviolet lointain est exigeante du point de vue instrumental (Moos et al. 2000), car la faible réflectance des couches optiques, dans cette région du spectre électromagnétique, oblige à réduire le plus possible le nombre de réflexions. Cependant, pour avoir une bonne résolution, le rapport focal doit être d'au moins 5 afin de limiter les aberrations optiques. Ceci nécessiterait de très longs instruments et de très grands réseaux de diffraction, ce qui cause évidemment problème pour un télescope spatial. Ce problème est résolu en remplaçant l'unique miroir primaire par plusieurs éléments optiques séparés.

L'instrument de FUSE est donc composé de quatre canaux (SiC 1, LiF 1, SiC 2, LiF 2; figure 1.1), chacun avec son propre miroir primaire de 352 x 387 mm d'une longueur focale de 2245 mm (Moos et al. 2000). Deux de ces miroirs sont recouverts de carbure de silicium (SiC) et les deux autres ont une couche d'aluminium recouverte de fluorure de lithium (LiF). Chacun des canaux se voit également assigné un réseau de diffraction de surface sphérique de rayon de courbure de 1652 mm.

FUSE est donc formé de deux paires de canaux identiques; cependant les canaux similaires (p.ex., SiC 1 et SiC 2) sont légèrement décalés en longueur d'onde afin de combler la partie du spectre (d'une largeur de ~10 Å) qui est coupée par une grille anti-ions située juste au-dessus des détecteurs et qui, par le fait même, sépare chaque

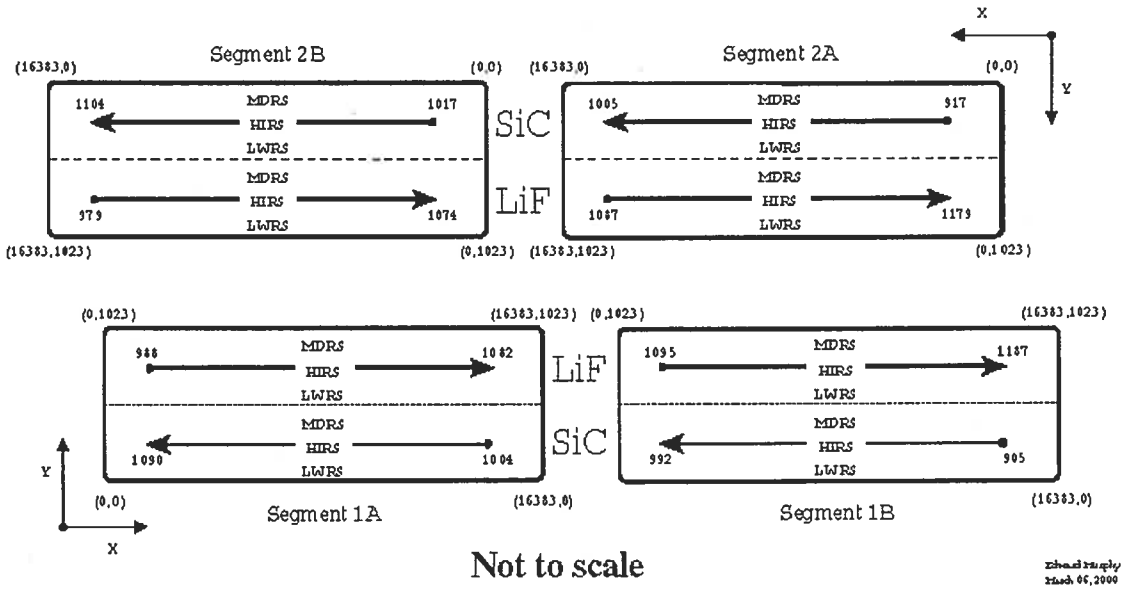

FIGURE 1.2 – Schéma représentant la disposition des détecteurs et leur couverture en longueur d'onde.

spectre en 2 segments (p.ex., SiC 1A et SiC 1B, SiC 2A et SiC 2B, etc.). La nature différente des miroirs permet d'observer des régions du spectre légèrement différentes (Figure 1.3). Une région spectrale donnée peut donc être couverte par un nombre de canaux différent d'une autre région.

Détecteur	Segment A (Å)	Segment B (Å)
SiC 1	1090.9 - 1003.7	992.7 - 905.0
LiF 1	987.1 - 1082.3	1094.0 - 1187.7
SiC 2	916.6 - 1005.5	1016.4 - 1103.8
LiF 2	1181.9 - 1086.7	1075.0 - 979.2

FIGURE 1.3 – Couverture en longueur d'onde des détecteurs.

De plus, l'aire effective de chacun des miroirs varie beaucoup en fonction de la longueur d'onde (Figure 1.4). Certains canaux offrent donc un meilleur rapport signal sur bruit (S/N) pour une région donnée.

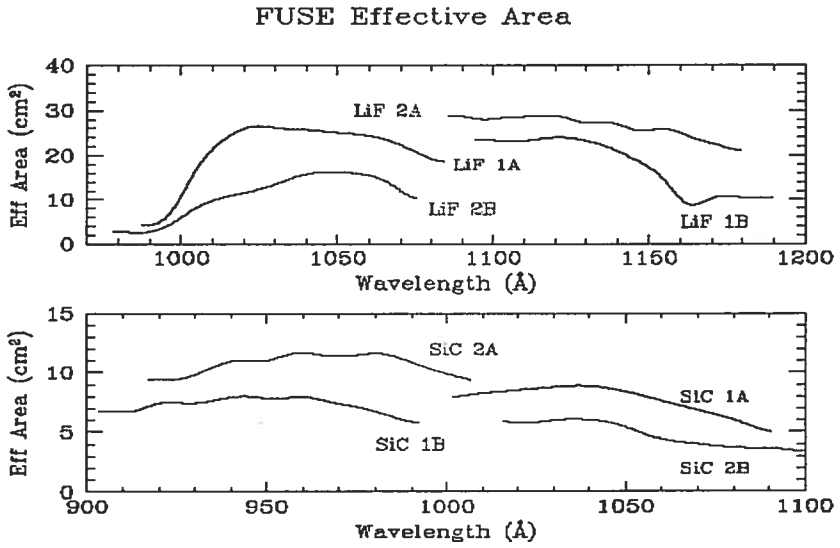

FIGURE 1.4 – L'aire effective des différents miroirs en fonction de la longueur d'onde.

Chapitre 2

Article

FUSE Observations of DB White Dwarfs[1]

N. Petitclerc, F. Wesemael

Département de Physique, Université de Montréal, C.P. 6128, Succ. Centre-Ville, Montréal, Québec, Canada H3C 3J7

nicolas, wesemael@astro.umontreal.ca

J.W. Kruk, P. Chayer[2]

Department of Physics and Astronomy, The Johns Hopkins University, Baltimore, MD 21218

kruk, chayer@pha.jhu.edu

M. Billères

European Southern Observatory, Santiago Headquarters, Avenida Alonso de Cordova 3107, Vitacura, Casilla 19001, Santiago 19, Chile

mbillere@eso.org

[1]FUSE is operated by John Hopkins University under NASA contract NAS 5-32985.

[2]Permanent affiliation: Department of Physics and Astronomy, University of Victoria, Victoria, BC, Canada V8W 3P6

2.1 Abstract

We present a comprehensive analysis of the far-ultraviolet spectra of three DB white dwarfs secured with the FUSE observatory. Transitions associated with various carbon ions are detected in all three objects. Atmospheric parameters are first redetermined on the basis of an analysis of archival data available, and the abundance of carbon, together with upper limits on the abundances of other heavy elements, are determined from the FUSE spectra. The log (C/He) ratios cover the range between -5.5 and -6.0. The presence of carbon, now detected in five DB stars with effective temperatures above 20,000 K, cannot be accounted for easily by physical processes currently thought to operate in the envelopes of DB stars. We suggest that a weak stellar wind threading the outer stellar layers of DB stars might sufficiently disrupt the settling of carbon leftover from the PG1159 phase to account for the carbon seen in the ultraviolet spectra of these objects.

2.2 Introduction

The DB white dwarfs belong to the subgroup of white dwarf stars whose optical spectrum is dominated by strong He I lines; these stars have long been known to possess an atmosphere composed of neutral helium to a high degree of purity. They represent less than 20% of the white dwarfs population and their effective temperatures range from 30,000 K to approximately 13,000 K. Because of the relative rarity of DB stars compared to their hydrogen-line counterparts, they are, on the average, fainter than DA stars and have consequently remained less amenable to detailed analyses than their counterparts. Some recent spectroscopic analyses (e.g., Beauchamp et al. 1996; Friedrich et al. 2000) have nevertheless gone some way toward a more complete understanding of the DB stars.

The purity of the photospheres of DB white dwarfs, where the abundance of helium generally exceeds that of any other chemical element by a factor $\gtrsim 10^5$ poses distinct challenges to theories of spectral evolution. On the one hand, hydrogen, lighter than helium, is expected to float at the top of the photosphere if present in significant abundance. On the other hand, the traditional heavy elements observed in white dwarf photospheres, like calcium, carbon, or silicon, are expected to sink in a helium-dominated atmosphere. Thus, in a DBZ white dwarf, one must explain both the absence of hydrogen and the presence of heavy elements, all the while calling on as few physical mechanisms as possible.

Carbon plays a special role among the heavy elements occasionally observed in helium-rich white dwarfs. It is observed in helium-atmosphere objects below $\sim 11,000$ K, either in the form of broad molecular bands in the optical spectrum of the DQ stars, or in the form of narrow transitions of C I in the ultraviolet spectrum of some DC stars. In contrast to the other heavy elements observed, which are thought to originate with accretion from the interstellar medium, it is thought that carbon originates from the deep regions of the stellar envelope, and is brought back to the surface by way of a complex dredge-up mechanism which digs into the carbon equilibrium diffusion tail below the helium convection zone (Koester et al. 1982; Fontaine et al. 1984). However, the efficiency of that mechanism is expected to decrease dramatically at effective temperatures above 13,000 K (Pelletier et al. 1986; MacDonald et al. 1998); above that threshold, the receding helium convection zone becomes too shallow for large quantities of carbon to be dredged-up in the photosphere.

Two investigations have contributed to documenting the pattern of carbon abundances in the photospheres of DB stars. The pioneering work of Wegner & Nelan (1987) was the first to provide upper limits on the C/He ratio in DB stars on the basis of the absence of C I transitions in low-dispersion IUE spectra of a sample of these objects. More recently, Provencal et al. (1996, 2000) have secured GHRS observations of three

DB stars and obtained the first determinations of the abundance of carbon in DB stars: these values, $-6 \lesssim \log \mathrm{C/He} \lesssim -5$, do not square well with the predictions of the standard dredge-up mechanism, and apparently require us to call upon new processes to maintain a measurable abundance of carbon in the photosphere of DB stars. Given the small number of objects observed, however, our picture of the abundance patterns of this trace element remains incomplete. An efficient way to move forward, however, is to use the FUSE satellite to observe DB stars in the 910-1185 Å range. There, 6 relatively strong carbon lines of 3 different ionization states are present and allow us to determine self-consistent values of the carbon abundance. Furthermore, this spectral range also includes many strong resonance transitions of several other heavy elements, which can be used to determine, or set upper limits on, the abundance of these elements.

In this initial contribution, we consider the problem of the abundance of trace elements in the photosphere of three DB white dwarfs. The first one, GD 190 (WD 1542+182), is a fairly bright (V=14.71) classical DB star. Its optical spectrum, characterized by strong He I lines, was the first observed to show the forbidden λ4517 component (Liebert et al. 1976). Since that time, it has been included in the analyses of Oke et al. (1984), Liebert et al. (1986), Wegner & Nelan (1987), and Thejll et al. (1991). GD 190 was included in the extensive spectroscopic analysis of Beauchamp et al. (1999) and was also part of the Provencal et al. (2000) sample: the GHRS data reveal photospheric C I and C II features in its far-ultraviolet spectrum. The second object is BPM 17088 (WD 0308−566), a bright ($V = 14.07$) unassuming southern DB star included in the investigations of Koester et al. (1981); Liebert et al. (1986); Wegner & Nelan (1987) and Thejll et al. (1991). The final star in our sample is EC 20058−5234 ($V = 15.58$), a V777 Her star discovered in the Edinburgh-Cape survey (Koen et al. 1995), and analyzed in a crude way by Beauchamp et al. (1999). That star, the hottest in the FUSE sample, has not been extensively analyzed since.

The aim of this paper is to determine or constrain the abundance of heavy elements,

in particular carbon, in the photosphere of these three DB stars. To do so, however, first requires values of the fundamental parameters of our target stars, namely effective temperature, surface gravity and hydrogen abundance. This investigation thus also provides a reconsideration of these parameters on the basis of all available data. We present the observational material which constitutes the backbone of this investigation in § 2. In § 3, we discuss the atmospheric models used, and present our analysis of the atmospheric parameters. Our abundance analyses are then presented in § 4, which also features a discussion of the possible origins of the observed carbon and our conclusions.

2.3 Observational material

2.3.1 FUSE data

The FUSE observatory produces high resolution spectra that range from 912 to 1187 Å, a region well suited to the search of weak lines associated with trace elements in the atmospheres of DB white dwarfs. The spectra analyzed here are all secured from the FUSE archive, and have two distinct origins: GD 190 and BPM 17088 were both observed within the photometric calibration program M102 proposed by one of us (JWK). The observations were carried out in TTAG mode with the large aperture (LWRS), a combination which provides a wavelength dependent resolution R $\sim$ 15,000. The third object was observed within program C046 (J.L. Provencal, PI), and was retrieved from the public MAST (Multimission Archive at Space Telescope) archives. The FUSE observation log for these three target stars is presented in Table 1.

The observation of GD 190 was carried out on 2001 March 29 and April 15 for a total integration time of 25,765 s. The data are reduced with the pipeline software CALFUSE (version 3.0.4), and provide a spectrum with a good S/N ratio for a star of that magnitude ($V = 14.71$). We co-add the 13 exposures for segments a and b of

each channel (LiF1, LiF2, SiC1, SiC2) individually. In our line analysis, we use the segment with the best effective area available for a given region. We also co-add the channels to produce a final spectrum covering the entire FUSE wavelength range with a optimal S/N ratio (Fig. 1). To do so, we linearly interpolate the spectra to generate a uniform wavelength grid with one flux point every 0.02 Å to preserve approximately the sampling of the individual spectra, which is now considerably reduced since version 3.0.0 of the pipeline. We then weigh the flux of each spectrum by the wavelength dependent effective area of the channels. Since FUSE uses the LiF1 channel for fine guidance, this channel is considered to have the best absolute wavelength scale. We therefore use the C II λ1037 doublet present in every channels to align the tree other channels with LiF1. We also remove the portion of the LiF1 channel spectrum which presents an abnormal flux level (the so-called "worm"). The noise level varies throughout the spectrum, since wavelength regions are covered by different numbers of detectors. The best exemple of this is seen around 1085 Å, were there is a gap between LiF channels. The co-addition process also averages the flux level of the different channels, but may degrade slightly the resolution of the resulting spectrum (e.g., Savage et al. 2002) Securing the best resolution is not an essential ingredient here, since we use this combined spectrum solely to extend the energy distribution of GD 190 into the far ultraviolet, in order to combine it with IUE and optical (spectro)photometric data.

BPM 17088 was observed on 2002 September 20, for a total integration time of 24,470 s. However, roughly a quarter of this observation time was lost for LiF1 and SiC1 due to a detector HV shutdown. The CALFUSE pipeline version 3.0.4 was used to reduce the data. We co-add all the valid exposures to secure a spectrum with a good S/N ratio for most channels, but only use the spectra of the channels with the best S/N ratio for our line analysis. However, we co-add the spectra of the different channels to get a final spectrum covering the whole FUSE wavelength range, as we did for GD 190.

EC 20058−5234 was observed on 2002 April 13 for a total of 20,840 s in TTAG mode

through the LWRS aperture. We treat these data in the same way as the other two objects (using the CALFUSE pipeline version 2.4.1), but co-add the different channels with a sampling of 0.006 Å. We find a clearly abnormal flux level in all five exposures in the SiC1a and SiC1b channels, probably caused by a misalignment of the target. The SiC1 channel is thus excluded from the channel coadddition.

2.3.2 HST GHRS data

GD 190 has previously been observed with the Goddard High Resolution Spectrograph (GHRS) on board HST, and these data were first analyzed by Provencal et al. (2000). The data were retrieved for this project from the MAST archives, and consist of two spectra: the first centered at 1215 Å, which covers the Lyα line, and the second centered at 1330 Å, which covers the C II λ1323, C I λ1329 and C II λ1335 lines (Figure 2). Exposure times are 3481.6 s for the former spectrum, and 4134.3 s for the latter. Both spectra were secured with the G160M grating, and are characterized by a dispersion of 0.07 Å per diode. The data centered on 1330 Å has since been rediscussed by Dufour et al. (2002).

2.3.3 IUE spectrophotometry

Both GD 190 and BPM 17088 were observed with the IUE, and were included in the initial analysis (Liebert et al. 1986) and later reanalysis (Thejll et al. 1991) of IUE observations of DB stars. The recalibrated low-dispersion, large aperture data were retrieved from the IUE Low Dispersion Archive created by Holberg et al. (2003). The effective exposure times in the SWP range (1200-2000 Å) were of 17,200 s for GD 190 and of 3,900 s for BPM 17088. In the LWR range (2000-3200 Å), the effective exposure times were of 7,200 s for GD 190 and of 4,500 s for BPM 17088. The spectral resolution is somewhat wavelength dependent and varies, for the LWR and SWP cameras, from 5

to 8 Å throughout the spectra. Our models were convolved with a 7 Å FWHM gaussian to reflect this limited resolution.

2.3.4 Optical spectroscopy

Because the determination of the abundances of trace elements depends on atmospheric parameters of our objects, it is of some value to constrain those as much as possible prior to the analysis of FUSE data. For this, we have relied both on our observational material (for GD 190 and, to some extent, for EC 20058−5234) and on archival data for all three targets secured within the SPY (SNe Ia Progenitor surveY) project.

The SPY project consists of a large survey for radial velocity variations in white dwarfs (Napiwotzki et al. 2001). Within it, a large numbers of white dwarfs were surveyed spectroscopically in a uniform manner. All observations were made with a high resolution spectrograph UVES (UV-Visual Echelle Spectrograph) at the ESO VLT in Chile. The SPY catalog happily includes optical spectra for all three of our objects. The UVES data are available on the ESO/ST-ECF (Space Telescope - European Coordinating Facility) Science Archives Facility and were secured by one of us (MB). The archive gives access to both the raw data and calibration files produced in a semi-automated way at Garching. These calibration files are produced by the UVES pipeline Data Reduction Software (DRS) developed by ESO. The pipeline is available to the public and is required to reduce the spectra from the calibration files. It is based on ESO-MIDAS (ESO - Munich Image Data Analysis System) which is also freely available. We created our own reduction blocks to reduce the spectra using version 2.0.0 of the pipeline. We then flux calibrated the spectra following the recipe given by ESO,[3] using IDL. The flux calibration is not carried out in the conventional way, using a standard star, but uses files created by ESO. These MASTER_RESPONSE files contain the wavelength dependent sensitivity of the detectors for every instrumental setup for a given period.

[3]http://www.eso.org/observing/dfo/quality/UVES/qc/response.html

It is created by daily observations of a set of standard stars.

The UVES spectra can reach a resolution of $\sim$ 110,000 with a narrow slit. But within the SPY project a wide slit is used (2.1″) to minimize slit losses, and this degrades the spectrum resolution to at least R $\sim$ 18,500 over the spectrum. The light is collected simultaneously on 3 CCDs which cover the following wavelength regions: 3290 to 4510 Å, 4620 to 5590 Å and 5675 to 6650 Å. The reader is referred to Koester et al. (2001) and Napiwotzki et al. (2001) for more details on the instrumental setup used for these observations.

The available data on GD 190 come from two sources. The object was first included in a sample of nearly 80 DB stars observed at the Steward Observatory 2.3-m telescope. The instrumental setup includes a Boller & Chivens Spectrograph, a 4.5 arcsec slit, and a 600 l mm^{-1} grating in first order. Together with a 800 $\times$ 800 TI or a 1200 $\times$ 800 Loral CCD, this combination provides coverage of the $\sim$ 3750 $-$ 5100 Å region at an intermediate resolution of $\sim$ 6 Å. Its spectrum is characterized by a S/N ratio of $\sim$ 80. It was also included in a sample observed at Hα and analyzed by Hunter (2001). The red spectroscopy was secured during a run at the 4m Mayall telescope at KPNO on 2000 February 22. Coverage extends approximately from 5600 Å to 7400 Å, at a resolution of at a resolution of $\sim$ 3 Å and a S/N ratio of $\sim$ 75. GD 190 was also observed within SPY, and a 300 s observation taken on 2003 April 23 was available from the archives. It was reduced in order to check for self-consistency with the earlier Steward Observatory and KPNO spectra. For BPM 17088, only SPY data were at our disposal, namely two short observations of 300 s, one secured on 2001 October 30 and the other on 2002 September 14. The two expositions for the red and blue segments are coadded and weighted by their S/N ratio. For our third target, a blue spectrum affected by some instrumental problems was used in a preliminary analysis by Beauchamp et al. (1999). That southern star was also observed within SPY on 2001 July 1: five expositions were taken for a total integration time of 16,500 s. The blue section of the spectra is reduced

successfully. Unfortunately, three of the available spectra show what appears to be a severe and problematic loss of light in the blue and are left out of our final spectrum. Furthermore, we are not able to reduce properly the red part of the spectrum, since the instrument setup is non standard and yields a spectrum characterized by a central wavelength of 6500 Å, which is not supported by the pipeline and for which no response curve for flux calibration exists. This is most unfortunate, given the problems already encountered by Beauchamp et al. (1999) in analyzing this star.

The reduction pipeline used with SPY data produces some known artifacts (Napiwotzki et al. 2001) in the spectra, like the sag in the 4250-4350 Å region (Figure 3) and the quasiperiodic pattern seen in the red spectrum of BPM 17088 in Figure 4. In general, we closely follow the procedure of Koester et al. (2001) in eliminating regions which include instrumental artifacts from our fits and benefit, to do so, from the lower resolution data available for GD 190, which is also shown in Figures 3 and 4.

2.3.5 Photometry

We use various photometric data to extend the energy distribution of GD 190, BPM 17088 and EC 20058−5234 into the optical range. For GD 190, we use multichannel observations from Greenstein (1984), which are on the AB79 scale. Since BPM 17088 is at a declination of −56°, there are no multichannel data available, and we use the numerous Strömgren data provided by Koester & Weidemann (1982), Bessell & Wickramasinghe (1978), and Wegner (1979). We average the magnitudes reported to find $y = 14.07$, $b = 14.38$ and $u = 14.005$. For the conversion of magnitudes to flux, we use the calibration of colors given by Heber et al. (1984). For EC 20058−5234 we use the corrected Johnson magnitudes from Koen et al. (1995) while, for flux calibration, we use the U,B,V,R,I zero points from Zuckerman et al. (2003).

The calculation of the theoretical flux in a given filter, required to fit the energy

distributions, is carried out in the manner described by Bergeron et al. (1995). For the multichannel system, we simply average the model fluxes in a 80 Å bandpass for the U, B, G and V filters and in a 160 Å bandpass for R and I. For the Strömgren system, we integrate the theoretical fluxes over the filter bandpasses of Olson (1974) while, for the Johnson system, we use the bandpasses UX, BX, B, V, R and I from Bessell (1990).

2.4 Atmospheric Parameters

2.4.1 Models

The grid of models and synthetic spectra used in this work are updated versions of those used in our previous analyses, in particular that of Beauchamp et al. (1999). These models are in LTE, are line-blanketed, and include convective energy transport. The chemical composition includes a variable H/He ratio. The calculations of the synthetic He I line spectrum take into account both van der Waals and resonance broadening at low effective temperatures, as well as the quadratic (and linear) Stark effect, which dominate in the hotter stars. We include the transition from impact to quasi-static broadening by the electrons, while the ions are always treated within the quasi-static approximation. Our analyses of the optical spectra of our target stars rely on these models.

For the abundances of heavy elements determined here, we use detailed synthetic spectra calculated by the publicly available code SYNSPEC (Hubeny & Lanz 1995). We use version 43 of the code. Our approach consists of treating the heavy elements as trace species and of feeding the temperature stratification provided by our own LTE code to SYNSPEC. The latter, in turn, calculates the LTE populations of the required ionization and excitations states as well as a line profile for the transitions of interest. As a final step, we convolve the synthetic spectra with a Gaussian of full width at half

maximum of 0.06 Å for the FUSE data sets and of 7 Å for the IUE data.

2.4.2 Photospheric and interstellar hydrogen

For GD 190, the availability of both the Lα line, in the GHRS spectrum, and the higher members of that series, from the FUSE spectra, makes the exercise of separating the photospheric from the interstellar components of the Lyman lines particularly interesting. For the Lα line, our procedure follows closely that of Provencal et al. (2000), which relies on a match to the line core to constrain the hydrogen column density and on a fit to the line wings to constrain the photospheric hydrogen abundance. The ISM absorption line profile is modeled by a damping profile (Spitzer 1978),

$$\tau_\nu = \tau_0 H(a,v) = \Big(\frac{1.497 \times 10^{-15} N_H \lambda_0 f_{ij}}{b}\Big) H(a,v)\,, \tag{2.1}$$

where N_H is the hydrogen column density in cm^{-2}, λ_0 and f_{ij} are the central wavelength in Å and oscillator strength of the transition, b is the ISM velocity dispersion in km s^{-1}, and a and v are the standard parameters of the Voigt profile. Since the line is saturated, the column density derived is essentially independent of the value of b. We find (Fig. 5) that the observed Lα feature can be well fit with a hydrogen column density of log $N_H = 18.5 \pm 0.1$ and that the photospheric hydrogen abundance must be small. This is consistent with the fact that no strong line asymmetry, caused by a Doppler shift between the ISM and photospheric components, is observed in the wings. The final photospheric abundance ratio is obtained by fixing the effective temperature and gravity at $T_{\rm eff} = 22,000$ K and log $g = 8.00$.

We measure the ISM velocity, $v_{\rm ISM} = -25.6\,{\rm km\,s^{-1}}$, on the basis of the N I triplet λ1220 in the GHRS spectrum centered at 1330Å. A consistent value, $v_{\rm ISM} = -23.7\,{\rm km\,s^{-1}}$, is obtained from the N I λ1134 triplet on the LiF segments. On the GHRS spectrum, we measure in addition the photospheric velocity on the basis of the

carbon lines, and find an average value of +23.4 km/s. These measurements imply a wavelength shift $\Delta\lambda \sim 0.2$ Å between the ISM and photospheric components in the GHRS spectrum centered at 1330Å. As mentioned earlier, the presence of a photospheric component would be mostly noticeable in the wings of the Lα line. Our overall best match to the line profile is secured for $18.4 \leq \log N_H \leq 18.6$ and $\log \mathrm{H/He} \leq -5.5$. Note that, given the uncertainties on N_H, the noise level of the spectrum, and the very weak sensitivity of our models to hydrogen abundances below $\log (\mathrm{H/He}) = -5.5$, our limits are less stringent than, but nevertheless consistent with, those proposed by Provencal et al. (2000), namely $\log (\mathrm{H/He}) \leq -6.5$ for $18.6 \leq \log N_H \leq 18.7$.

The FUSE spectra contain several additional Lyman lines originating in the ISM: about twenty such lines can be identified toward the the Lyman jump. The first four lines Lβ-Lϵ ($\lambda\lambda$1025.72, 972.54, 949.74 and 937.8) are severely contaminated by airglow emission, but all lines originating from higher levels appear free from geocoronal contribution. The higher lines are covered by the SiC2a and SiC1b segments but, since the SiC2a has a larger effective area, we used the five uncontaminated lines it contain, namely $\lambda\lambda$930.75, 926.23, 923.15, 920.96 and 919.35, to constrain the hydrogen column density toward GD 190 and BPM 17088. To do so, we use FSIM, an IDL based set of routines provided by the FUSE observatory. In contrast to Lα, the ISM lines are not saturated, and the adopted value of the Doppler broadening parameter b is of critical importance. We find a difference of many orders in column density for calculations with a b ranging from 10 to 5 km/s. For the default FSIM value of $b = 10$ km/s, we find $\log N_H = 18.0 \pm 1$ for GD 190, fairly close to the value found with the Lα, whose width depends little on the value of b. In BPM 17088, the same procedure suggests a much larger ISM column density, $\log N_H = 20.0 \pm 1$.

2.4.3 Optical spectrum analysis

The atmospheric parameters of GD 190 have been the subject of several investigations. Our starting point are the recent values of Beauchamp et al. (1999), who analyzed a blue, optical spectrum at intermediate ($\sim$ 6Å) resolution to determine $T_{\rm eff} = 21,500$ K and $\log g = 8.00$ on the basis of models devoid of hydrogen, and $T_{\rm eff} = 21,000$ K and $\log g = 8.03$ on the basis of models with the largest traces of hydrogen allowed by the non visibility of the Hβ and Hγ lines, namely log (H/He)~ -4.5. Subsequently, Provencal et al. (2000) secured an independent estimate of the effective temperature on the basis of the strength of the carbon lines, and obtained $T_{\rm eff} = 23,000 \pm 1000$ K, while Hunter (2001) refined the upper limit on the hydrogen abundance at log (H/He) < -4.8 on the basis of the absence of the Hα line in the medium-resolution ($\sim$ 3Å) red optical spectrum he analyzed.

The analysis of the archival blue and red UVES spectra with our updated model grid provides independent estimates of these parameters and a measure of the external error on the difficult determination of the atmospheric parameters of DB stars; we find that the hydrogen abundance satisfies log (H/He) < -4.75, a value consistent with the Hunter (2001) result, and an effective temperature and surface gravity of $T_{\rm eff} = 22,300$ K and $\log g = 7.98$. At the same time, our reanalysis of the intermediate-resolution spectrum of Beauchamp et al. (1999) with our current generation of synthetic spectra yields $T_{\rm eff} = 22,050$ K and $\log g = 7.97$ for the same hydrogen log (H/He) $= -4.75$. Overall, thus, an effective temperature of $T_{\rm eff} = 22,000 \pm 1000$ K appears to be consistent with our current analysis of the four optical data sets available.

BPM 17088, in contrast, has a sparser history and the archival blue and red UVES spectra represent the first opportunity to study spectroscopically this southern object in some detail. The high-resolution red spectrum shows no Hα line, and a direct comparison shows that GD 190 and BPM 17088 appear to have nearly identical optical

spectra. Our fits are consistent with an effective temperature and surface gravity of $T_{\rm eff} = 22,600 \pm 1000\,{\rm K}$ and $\log g = 8.13$, while a limit on the hydrogen abundance similar to that in GD 190 can be set at Hα, namely $\log ({\rm H/He}) < -4.75$.

For EC 20058−5234, the higher temperature and lack of coverage at Hα in the UVES data conspire to provide only a weak constraint on the hydrogen abundance, $\log ({\rm H/He}) < -3.50$, similar to that set by Beauchamp et al. (1999). Furthermore, the blue UVES spectrum, with its regions with instrumental artifacts removed, only provides an uncertain temperature based on isolated islands of flux. Meanwhile, our reanalysis of the (flawed) intermediate-resolution spectrum of Beauchamp et al. (1999) with our current generation of synthetic spectra yields a temperature consistent with, but hardly more accurate than, our earlier determination. On balance, thus, we feel we are not in a position to improve upon the analysis of Beauchamp et al. (1999), who place the temperature of EC 20058−5234 between 27,100 and 28,400 K. For the purpose of the carbon abundance determination, we use an uncertain effective temperature $T_{\rm eff} = 28,000\,{\rm K}$ for EC 20058−5234. The current status of this object is particularly unsatisfactory in view of its recently advertised importance as a test of microphysical processes (Winget et al. 2004).

2.4.4 Energy distributions

The complete energy distributions of GD 190 and BPM 17088 can be constructed by combining the coadded FUSE spectra displayed in Figure 1 with archival IUE and published photometric data. Because these energy distributions are sensitive to the effective temperature and interstellar reddening, they provide, when available, an important self-consistency check on our determinations of $T_{\rm eff}$ and of the hydrogen column density along the line of sight. In the case of EC 20058−5234, the absence of IUE data makes the exercise less compelling.

To construct the complete energy distribution, we first remove all strong airglow lines and strong ISM hydrogen absorption lines. We also bin the IUE and FUSE spectra in bins 10 Å wide. The theoretical energy distributions are calculated with our own LTE code, are at fixed $\log g = 8.0$ gravity, and include a small hydrogen abundance ($\log(\mathrm{H/He}) = -6.5$) and no heavy elements.

The optimal effective temperature is found by a χ^2 minimization, which also yields the solid angle. The three spectral regions (optical photometry, IUE and FUSE spectrophotometry) are given equal weight in the fits. Some allowance is made for possible reddening along the line of sight by using the hydrogen column densities determined on the basis of the FUSE spectra. These are converted to color excess with the use of the general relation of Spitzer (1978),

$$N_H = 5.9 \times 10^{21} E_{B-V} \,\mathrm{mag}^{-1}\,\mathrm{cm}^{-2}, \tag{2.2}$$

For GD 190, we derive a negligible color excess of $E_{B-V} = 0.00017$ mag, and our fit yields an optimal effective temperature of 22,600 K. For BPM 17088, we find a larger value of $E_{B-V} = 0.0017$ mag, and a temperature of 22,700 K. The values of the color excess we determine can be checked against the reddening maps of Burstein & Heiles (1982). For GD 190, located at $l = 29.49°$ and $b = 49.72°$, the maximum reddening tabulated is $E_{B-V} = 0.01625$, ten times higher than the value determined on the basis of the FUSE spectra; the use of this value in our fits leads to an effective temperature of 23,200 K. For this larger value, however, the extinction bump at 2200 Å should be apparent in the IUE spectrum, but is not. For BPM 17088, located at $l = 272.44°$ and $b = -51.75°$, the maximum reddening tabulated is identically zero. All available data point toward a very small color excess in the direction of these two targets. Were instellar reddening omitted altogether from our analysis, the derived temperatures would be 22,600 K for GD 190 and 22,100 K for BPM 17088 (Fig. 6), both within the

error bars of our optical determinations.

For EC 20058−5234, only optical photometry and FUSE data are available. Figure 7 suggests that a somewhat larger color excess appears required to fit the photometry as well as the slope of the FUSE spectrum continum. An acceptable fit is found with E_{B-V} = 0.05 and $T_{\rm eff}$ = 28,376 K. The freedom to consider higher values of the color excess is larger here since, in the absence of IUE data, there are no constraints coming from the the 2200 Å extinction bump. But the value we consider here for EC 20058−5234 is probably within the realm of possibilities, since this star has the lowest galactic latitude of our three program stars ($\ell = 346°$, $b = -33°$). Furthermore, the color excess we derive is in agreement with the value obtained from the reddening maps, which yield $E_{B-V} = 0.04825$ for that direction.

2.5 Results of abundance analyses

2.5.1 Carbon

The FUSE spectra of all three target stars are characterized by a hot stellar continuum on which appear several interstellar and photospheric lines (Fig. 1). Of particular interest to us are the detection of six lines of carbon: C I λ945, C II λ1010, λ1037, and λ1066, as well as C III λ977 and λ1176.

In GD 190, these lines complement the C I λ1329 and C II λ1324 and λ1335 transitions observed in the GHRS spectra by Provencal et al. (2000). A photospheric origin of the new FUSE detections at C II λ1010, λ1066, and C III λ1176 seems likely, since these transitions originate on excited states of their respective ions ($E_{\rm ex} > 5.3$ eV). For those lines in the FUSE spectra with components originating both on the ground state and on an excited fine-structure state, like C I λ945 and C II λ1037, the presence of an ISM component shifted by ~ 0.16 Å complicates the modeling of the line shapes (Fig.

8).

The similarity between GD 190 and BPM 17088, already noticed in the analysis of the optical spectrum and spectral energy distribution, extends to the FUSE range (Fig. 1). The strengths of the six photospheric carbon lines in these stars appears comparable. In BPM 17088,, the ISM N I λ1134 triplet is unusable because of geocoronal emission, but we estimate $v_{\rm ISM} = -9\,{\rm km\,s^{-1}}$ from the interstellar components of the C I λ945 and C II λ1037 transitions. Because the estimated photospheric velocity obtained from the same lines is $+59\,{\rm km\,s^{-1}}$, the ISM and photospheric components for the two transitions concerned are well separated. We note that BPM 17088 is included in the sample of hot stars in the galactic halo (under the name CS 22968−019) studied by Beers et al. (1992), who measure a photospheric velocity of $-68\,{\rm km\,s^{-1}}$ (the sign being a likely typo), while its radial velocity is also given by Wegner (1974) as $+61\,{\rm km\,s^{-1}}$.

Finally, in the spectrum of EC 20058−5234, the carbon features — in particular C I λ945, C III λ977 and C II λ1066 — appear substantially weaker than in the other two target stars. Here, we estimate $v_{\rm ISM} = -33\,{\rm km\,s^{-1}}$ from the interstellar component of the C II λ1037 transition and an average photospheric velocity, based on the three strongest carbon lines, of $+15\,{\rm km\,s^{-1}}$.

In GD 190, the carbon abundance determination relies on all nine lines associated with three ions. The C I λ945 and C II λ1066 lines currently appear to be the most useful effective temperature and abundance indicators. From the FUSE and GHRS ranges, we determine a carbon abundance of $\log({\rm C/He}) = -5.5 \pm 0.3$. The modeling of the resonance transitions C III λ977 and C II λ1037 requires that we include a shifted ISM component in the simulation, as shown in Figure 8. Our determinations are consistent with the value $\log({\rm C/He}) = -5.8 \pm 0.4$ favored by the Provencal et al. analysis of the GHRS data alone. Likewise, in BPM 17088, we find $\log({\rm C/He}) = -5.5 \pm 0.3$, while for EC 20058−5234 the optimal carbon abundance reads $\log({\rm C/He}) = -6.0 \pm 0.3$.

The current pattern of carbon abundances in helium-atmosphere degenerates is

shown in Figure 12, which builds on a similar figure displayed by Provencal et al. (2000). To generate the figure, we combine the carbon abundances determined here with those redetermined by Dufour et al. (2004) for two additional hot DB stars, GD 358 and PG 0112+104. We also use the since recalibrated archival low-dispersion IUE spectra (Holberg et al. 2003) of the large sample of DB stars observed by Wegner & Nelan (1987) to rederive upper limits on the carbon abundance in these objects. For this purpose, we do not redetermine the atmospheric parameters or the photospheric hydrogen abundance but rather use the original values of $T_{\rm eff}$, log g and H/He ratio used by Wegner & Nelan (1987). While our results are globally consistent with theirs, we tend to derive more conservative upper limits than they did, for example in the case of PG 1445+152 and GD 303 (WD 1011+570). These differences are likely to be due, in part, to the recalibration of the SWP images. On the cool side, the carbon abundances in the DQ stars come mainly from the published work of Wegner and of Zeidler, K.T. and their coworkers, whose values were used as published.

2.5.2 Other heavy elements

Carbon is ubiquitous in the photospheres of the DB white dwarfs we have observed, and the specific role played by this element within schemes of spectral evolution of white dwarfs will be considered in the next section. However, the spectral bandpass of the FUSE detectors also provides coverage of a number of lines of other heavy elements of interest. For example, upper limits on the abundances of Si, Mg and Fe in the photospheres of DB stars at or above $T_{\rm eff} \sim 20,000$ K can be secured from existing FUSE spectra. Our results for these three elements are presented in Table 2.

2.5.3 The origin of carbon

With the addition of BPM 17088 and EC 20058−5234, the tally of DB white dwarfs which display detectable abundances of carbon now reaches five. With the prospect of observing several additional stars with FUSE, it is likely that the pattern of abundance of that element in DB stars will be considerably clarified in a fairly short time.

Accounting for the carbon observed may provide an even more challenging task. Four ideas can be considered to account for its presence. At high effective temperatures, radiative forces are often called upon to account for the presence of heavy elements in white dwarf photospheres. In the simplest model, an equilibrium abundance of any element can be maintained in the atmospheric layers when the upward radiative acceleration compensates exactly the downward effective gravity, which combines the gravitational acceleration and that associated with the electric field in the plasma. The amount of radiative support in the photospheres of helium white dwarfs has been investigated by Vauclair et al. (1979) and Chayer et al. (1995). The Chayer et al. (1995) results show, in particular, that in a $T_{\rm eff} = 40,000$ K $\log g = 8.0$ model (a regime where there are actually no reported helium-rich stars), the equilibrium carbon abundance at the photosphere is down to log (C/He)= −5.0. At cooler temperatures, in the DB range of interest here, the developing convection zone guarantees a well-mixed envelope, and the diffusion velocities must be evaluated at the base of that zone, through which carbon is likely to settle rapidly. It thus appears unlikely that radiative support plays a significant role in maintaining the carbon abundances observed in our objects, a conclusion already reached by MacDonald et al. (1998) for the specific case of GD 358. A variation on that theme was brought up briefly by Provencal et al. (2000), namely that the observed carbon be brought up to the surface through additional mixing associated, perhaps, with stellar rotation; this option was shown to be inconsistent with our current knowledge of DB stars by Dufour et al. (2002).

At cooler temperatures, in the realm of the DQ stars, there is convincing evidence that the observed carbon is intrinsic, dredged-up from the tail of the carbon diffusion profile back to the photosphere by the deepening helium convection zone. The model, originally proposed by Koester et al. (1982) and Fontaine et al. (1984), has been quite successful in explaining both the amount of carbon pollution and its dependence on the effective temperature (Pelletier et al. 1986; MacDonald et al. 1998). However, it seems implausible that DB stars upward of 20,000 K could be polluted by this mechanism at the level observed ($-6 \lesssim \log \mathrm{C/He} \lesssim -5$) unless all DB stars have helium envelope masses that are over 10 orders of magnitude smaller than those favored by evolutionary models.

A third option is that the observed carbon originates from the interstellar medium, as do most of the heavy elements observed in cool white dwarfs. This option is strongly constrained by the fact that hydrogen does not appear to be an important chemical species in the atmosphere of the DB stars considered here. A standard way of accounting for the simultaneous absence of hydrogen and presence of accreted heavy elements, specifically carbon, is to call on a propeller-like model such as that adapted by Wesemael & Truran (1982); the model relies on a rotating magnetic field to bat away ionized hydrogen while allowing the heavy elements, locked up in grains, to cross the magnetosphere unimpeded and to evaporate within it. Few observational tests of this model exist, although this is changing slowly (Friedrich et al. 2003). For one of the DB stars for which carbon is observed, the V777 Her star GD 358, the input parameters have been estimated from asteroseismology. On that basis, MacDonald et al. (1998) argue that the strength of the average surface magnetic field ($1.3 \pm 0.3\,\mathrm{kG}$) and of the rotation period ($P = 0.89\,\mathrm{d}$) imply that the graphite grains should evaporate outside of the magnetosphere, and would suffer a fate similar to that of the hydrogen ions. While there is no easy way to estimate the required parameters for the other DB stars under study here, accretion does not appear to be a viable candidate as the source of carbon

in those stars.

Faced with this dearth of acceptable models, we propose that the carbon observed is intrinsic and is a leftover from the evolutionary connection which links the PG1159 stars first to the DO stars and later to the DB stars. As argued most recently by Dehner & Kawaler (1995) and Brassard & Fontaine (2002), the chemical separation of helium from carbon/oxygen is not completed by the time a cooling PG1159 descendant reaches the DB stage, and this may perhaps allow some residual carbon to be present in the envelope even by the time the progenitor has cooled to the DB range. Unfortunately, the resulting carbon abundance at the photosphere appears to be many orders of magnitude smaller than that observed in our three target stars, as diffusion is such an efficient mechanism in the upper layers. Thus, the calculations of Brassard & Fontaine (2003) show that, by the time the cooling PG1159/DO star reaches 30,000 K, the leftover photospheric C/He ratio is inferior to 10^{-15}, and in fact reaches a minimum in the effective temperature range where the carbon features are observed with FUSE. In many ways, this situation mirrors that observed in the DAO white dwarfs and in the sdB stars, where the efficient gravitational settling should lead to residual traces of helium many orders of magnitude smaller than are observed. The way out of this conundrum is similar to that proposed in the context of the DAO and sdB stars: a weak wind which pervades the atmosphere and envelope of the DO and DB stars and competes efficiently with the ongoing downward settling of carbon. The preliminary investigations of winds along the PG1159/DO/DB cooling track (Brassard & Fontaine 2004) is based on fully evolutionary models which include a wind whose mass loss rate decreases in a manner inversely proportional to the age and turns off by the time the DB star reaches 20,000 K. In the DB range, the mass loss rate is of the order of $\sim 10^{-13}\, M_{\odot}\, \mathrm{yr}^{-1}$, a value consistent with the rates discussed by Unglaub & Bues (2000). At this rate, the mass loss process impedes the downward settling of carbon and leads to photospheric C/He ratios in the DB range, log (C/He) ~ -7, substantially larger than predicted in windless models but consistent with the

abundances we measure in DB stars (Fig. 12). While this suggestion remains tentative, and these winds have yet to be observed, the idea appears most promising and needs to be explored in more detail.

From an observational perspective, it is important to continue the work initiated by Provencal et al. (2000) and pursued in this paper, namely the mapping of the carbon and hydrogen abundance patterns in DB stars. The work must also be extended to cooler DB stars, in which the mass loss rate may be expected to decrease and the wind could well turn off altogether. Observations of cooler stars may perhaps reveal the transition from a wind-dominated atmosphere to one where the dominant processes could be accretion of heavy-elements from the ISM and dredge-up of carbon from the deeper layers.

2.6 Acknowledgements

We are grateful to J.L. Provencal for securing the FUSE observations of EC 20058−5234, and to P. Brassard and G. Fontaine for informative discussions. This work was supported in part by the NSERC Canada and by the Fund FQRNT (Québec).

TABLEAU 2.1 – Log of FUSE Observations

Name	Program ID	Date	Aperture	MODE	Number of Exposures	Exposure Time (s)
GD 190	M1020201	2001-03-29	LWRS	TTAG	2	4722
	M1020202	2001-04-15	LWRS	TTAG	11	21043
EC 20058−5234	C0460201	2002-04-13	LWRS	TTAG	5	20841
BPM 17088	M1020401	2002-09-20	LWRS	TTAG	7	12345
	M1020402	2002-09-20	LWRS	TTAG	3	11550
	M1020403	2002-09-20	LWRS	TTAG	3	12843

TABLEAU 2.2 – Upper limits on the abundances of heavy elements

Name	Transition	log (Abundance/He)
GD 190	Si III λ 1108	< -8.5
	Mg II λ 947	< -4.5
	Fe III λ 1122	< -7.0
BPM 17088	Si III λ 1108	< -8.0
	Mg II λ 947	< -4.5
	Fe III λ 1122	< -7.0
EC 20058−5234	Si III λ 1108	< -7.5
	Fe III λ 1122	< -7.0

Bibliographie

Bibliography

Beauchamp, A., Wesemael, F., Bergeron, P., Liebert, J., & Saffer, R.A. 1996, in Hydrogen-Deficient Stars, eds. C.S. Jeffery & U. Heber, (San Francisco; A.S.P.), p. 295

Beauchamp, A., Wesemael, F., Bergeron, P., Fontaine, G., Saffer, R.A., Liebert, J. & Brassard, P. 1999, ApJ, 516, 887

Beers, T.C., Preston, G.W., Shectman, S.A., Doinidis, S.P., & Griffin, K.E. 1992, AJ, 103, 267

Bergeron, P., Wesemael, F., & Beauchamp, A. 1995, PASP, 107, 1047

Bessell, M.S. 1990, PASP, 102, 1181

Bessell, M.S. & Wickramasinghe, D.T. 1978, MNRAS, 182, 275

Brassard, P. & Fontaine, G. 2002, ApJL, 581, L33

Brassard, P. & Fontaine, G. 2003, in White Dwarfs, eds. D. de Martino, R. Silvotti, J.-E. Solheim, & R. Kalytis, (Dordrecht: Kluwer), p. 259

Brassard, P. & Fontaine, G. 2004, private communication

Burstein, D. & Heiles, C. 1982, AJ, 87, 1165

Chayer, P., Fontaine, G. & Wesemael, F. 1995, ApJS, 99, 189

Dehner, B.T. & Kawaler, S. 1995, ApJL, 445, L141

Dufour, P., Wesemael, F., & Bergeron, P. 2002, ApJ, 575, 1025

Dufour, P., Wesemael, F., & Bergeron, P. 2004, in preparation

Fontaine, G., Villeneuve, B., Wesemael, F., & Wegner, G. 1984, ApJ, 277, L61

Friedrich, S., Koester, D., Christlieb, N., Reimers, D. & Wisotzki, L. 2000, AA, 363, 1040

Friedrich, S., Jordan, S., & Koester, D. 2003, in White Dwarfs, eds. D. de Martino, R. Silvotti, J.E. Solheim & R. Kalytis (Dordrecht: Kluwer), p. 203

Greenstein, J.L. 1984, ApJ, 276, 602

Heber, U., Hunger, K., Jonas, G. & Kudritzki, R.P. 1984, AA, 130, 119

Holberg, J.B., Barstow, M.A. & Burleigh, M.R. 2003, ApJS, 147, 145

Hubeny, I. & Lanz, T. 1995, ApJ, 439, 875

Hunter, C. 2001, M.Sc. thesis, Université de Montréal

Koen, C., O'Donoghue, D., Stobie, R.S., Kilkenny, D., & Ashley, R. 1995, MNRAS, 277, 913

Koester, D., Schulz, H., & Wegner, G. 1981, AA, 102, 331

Koester, D. & Weidemann, V. 1982, Å, 108, 406

Koester, D., Weidemann, V., & Zeidler-K.T. 1982, Å, 116, 147

Koester, D. et al. 2001, AA, 378, 556

Liebert, J., Beaver, E.A., Robertson, J.W., & Strittmatter, P.A. 1977, ApJL, 204, L119

Liebert, J., Wesemael, F., Hansen, C.J., Fontaine, G., Shipman, H.L., Sion, E.M., Winget, D.E., & Green, R.F. 1986, ApJ, 309, 241

MacDonald, J., Hernanz, M., & José, J. 1998, MNRAS, 296, 523.

Napiwotzki, R. et al. 2001, AN, 322, 411

Oke, J.B., Weidemann, V. & Koester, D. 1984, ApJ, 281, 276

Olson, E.C. 1974, PASP, 86, 80

Pelletier, C., Fontaine, G., Wesemael, F., Michaud, G., & Wegner, G. 1986, ApJ, 307, 242

Provencal, J.L., Shipman, H.L., Thejll, P., Vennes, S., & Bradley, P.A. 1996, ApJ, 466, 1011

Provencal, J.L., Shipman, H.L., Thejll, P., & Vennes, S. 2000, ApJ, 542, 1041

Savage, B.D., Sembach, K.R., Tripp, T.M., & Richter, P. 2002, ApJ, 564, 631

Spitzer, L., Jr. 1978, Physical Processes in the Interstellar Medium (New York: Wiley)

Thejll, P., Vennes, S. & Shipman, H.L. 1991, ApJ, 370, 355

Unglaub, K. & Bues, I. 2000, AA, 359, 1042

Vauclair, G., Vauclair, S., & Greenstein, J.L. 1979, AA, 80, 79

Wegner, G. 1979, MNRAS, 166, 271

Wegner, G. 1979, AJ, 84, 1384

Wegner, G. & Nelan, E.P. 1987, ApJ, 319, 916

Wesemael, F. & Truran, J.W. 1982, ApJ, 260, 807

Winget, D.E., Sullivan, D.J., Metcalfe, T.S., Kawaler, S.D., & Montgomery, M.H. 2004, ApJL, 602, L109

Zuckerman, B., Koester, D., Reid, I.N., & Hünsch, M. 2003, ApJ, 596, 477

Chapitre 3

Figures

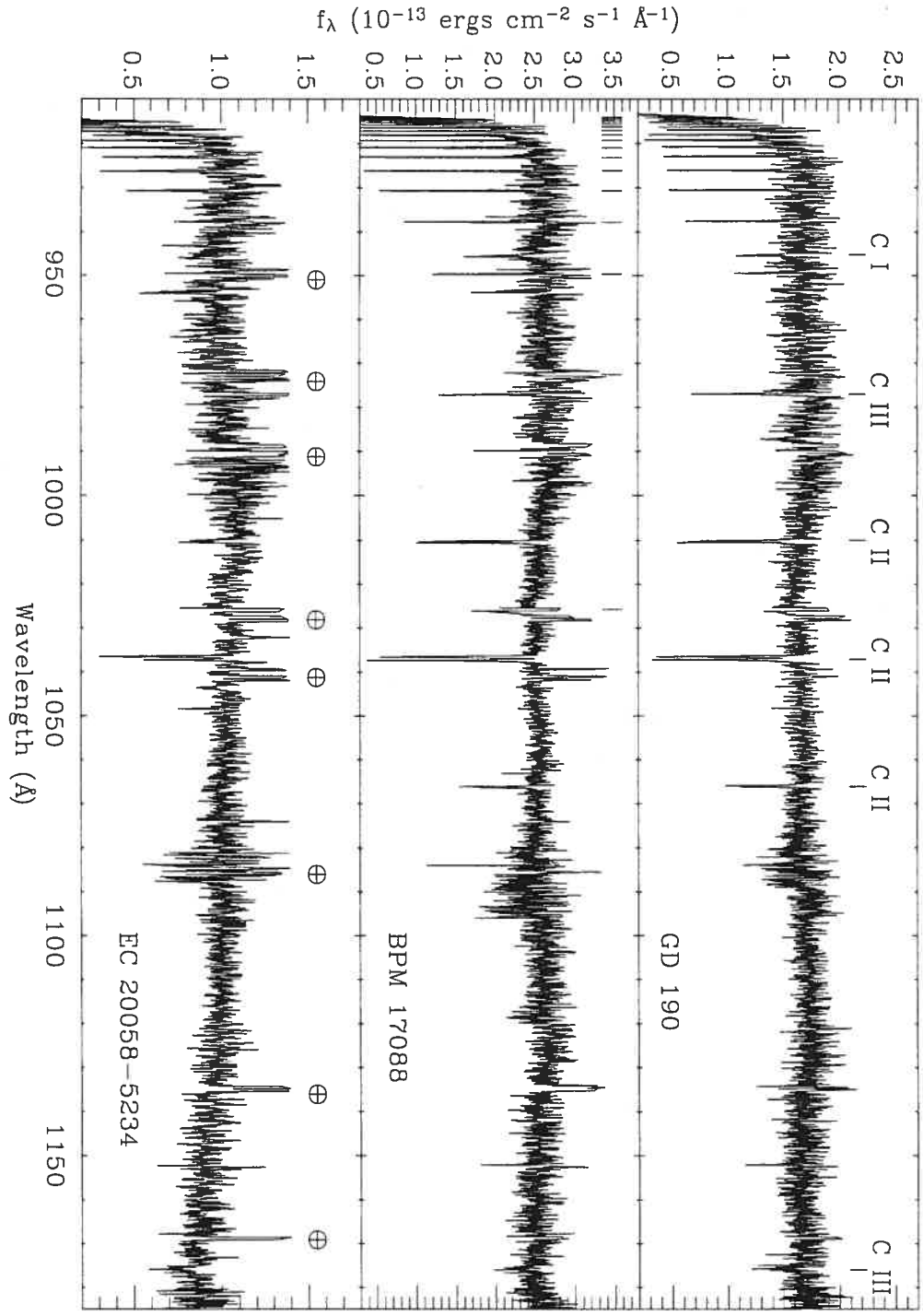

FIGURE 3.1 – FUSE spectra for all three target stars. In the top panel, the six carbon lines used in this investigation are labelled. In the middle panel, the location of the Lyman series originating in the ISM is marked. In the bottom panel, the location of the undesirable and removed airglow lines is indicated. Most of these features are present in the spectra of the three stars. The GD 190 and BPM 17088 spectra were smoothed with a 3-point average, that of EC 20058−5234 with a 21-point average.

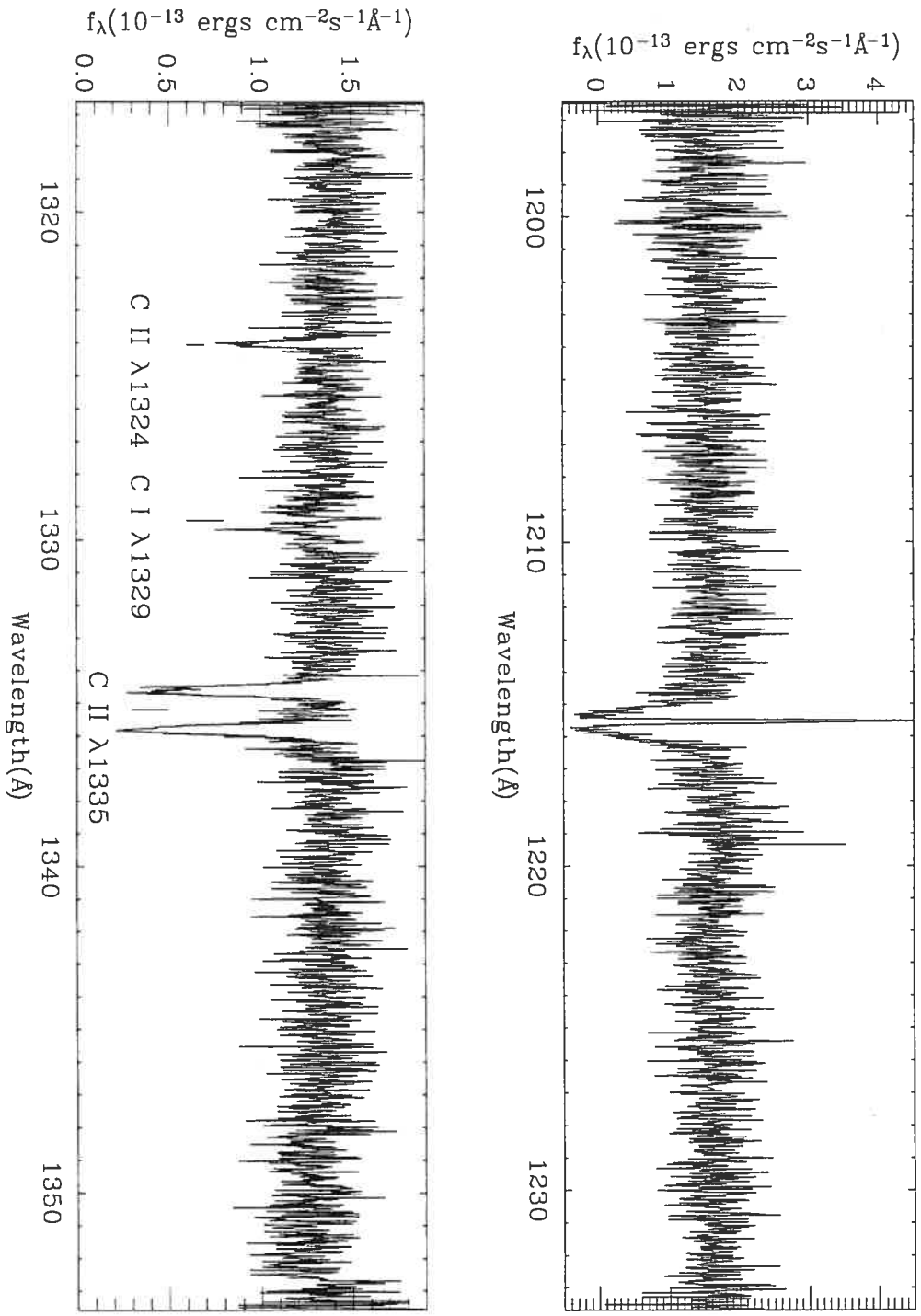

FIGURE 3.2 – Archival GHRS spectrum of GD 190. The top pannel shows the Lα profile, while the lower panel shows the three carbon transitions discovered by Provencal et al. (2000).

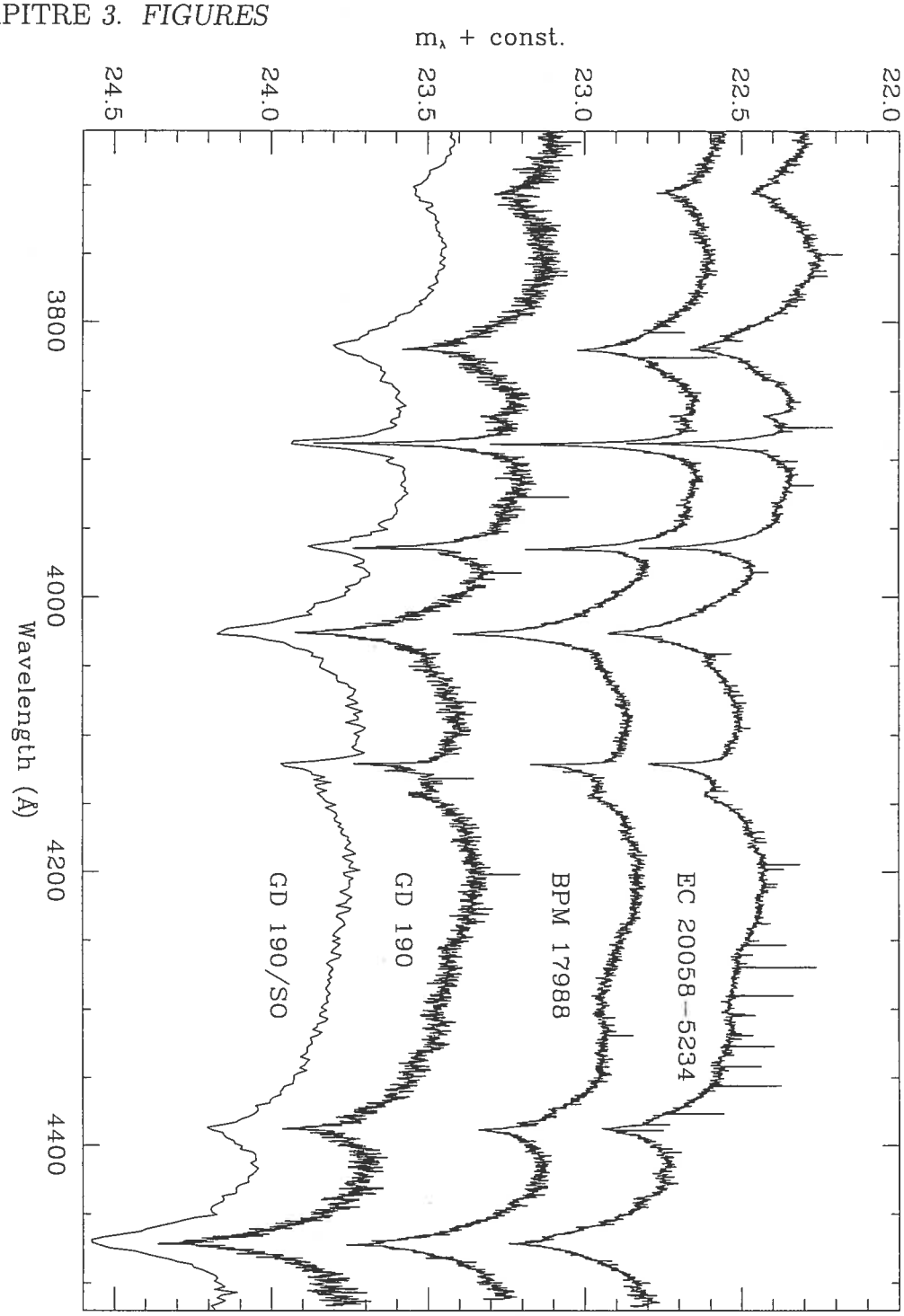

FIGURE 3.3 – Archival UVES blue spectra of out three target stars. The bottom spectrum, labeled SO, is a lower-resolution spectrum of GD 190 secured at the Steward Observatory and used for comparison.

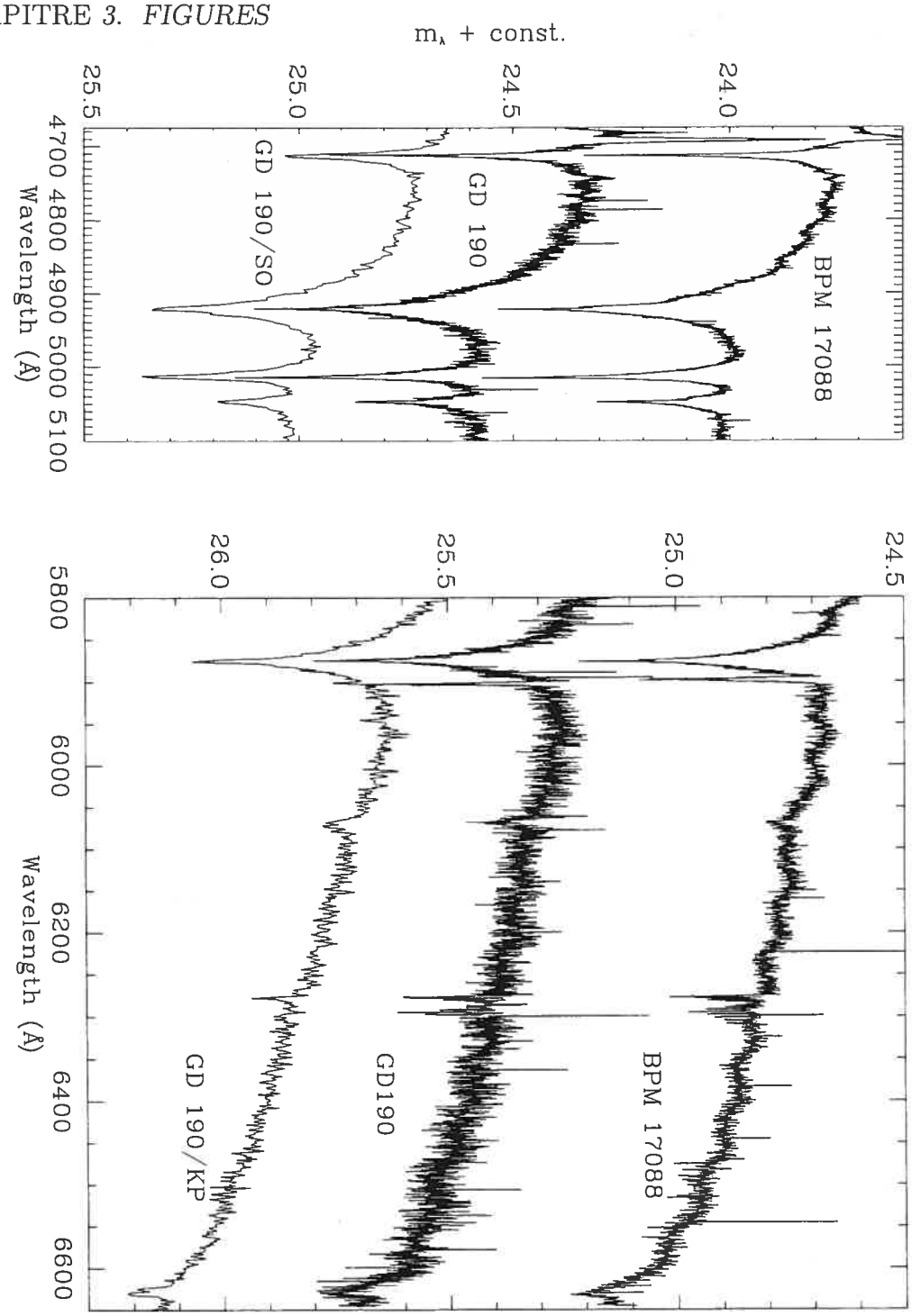

FIGURE 3.4 – Archival UVES red spectra for BPM 17088 (top) and GD 190 (middle). The bottom plots, labeled SO and KP, are lower-resolution spectra of GD 190 secured at Steward Observatory (left box; blue spectrum longward of 4700 Å) or at Kitt Peak National Observatory (right box; red spectrum) and used for comparison.

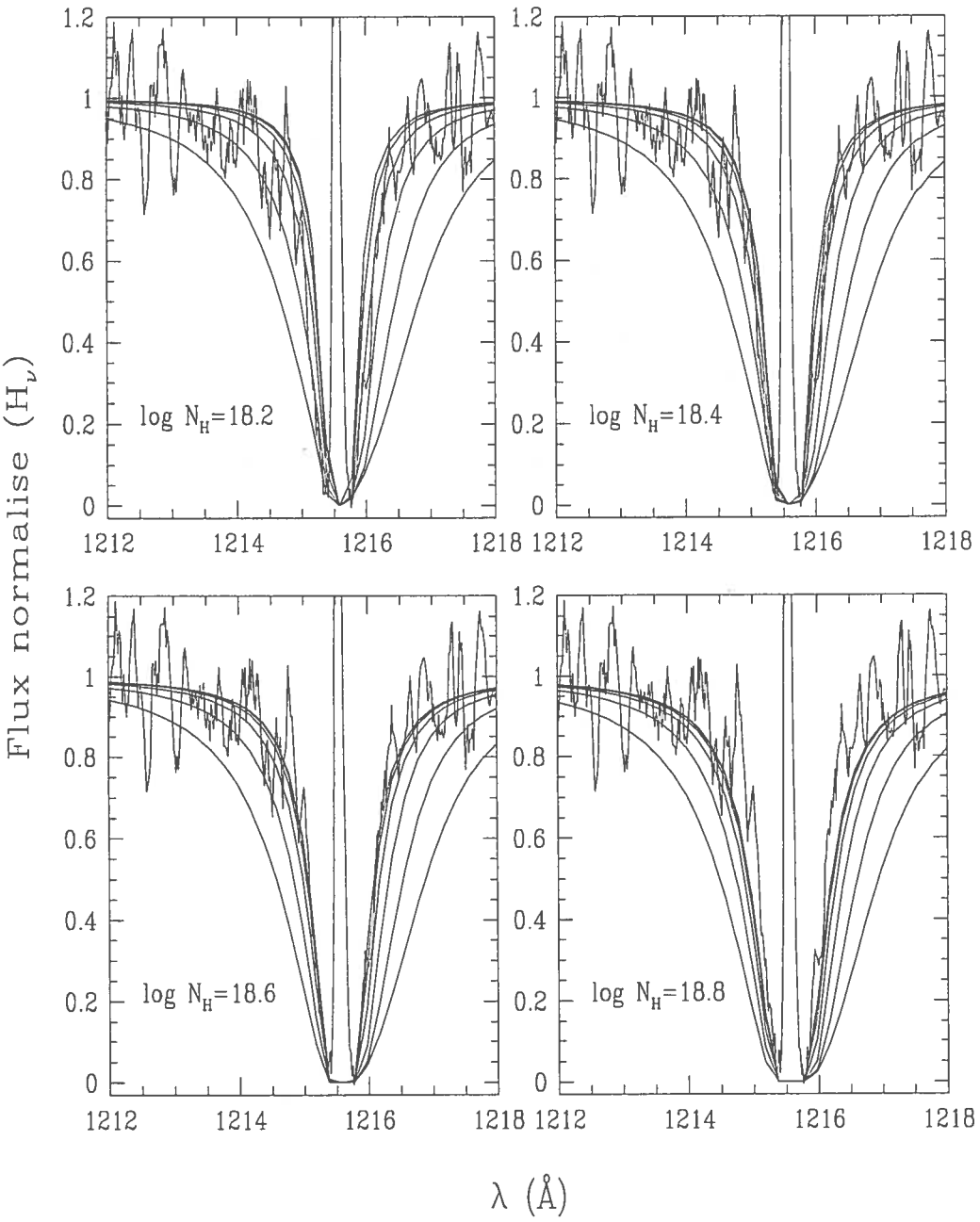

FIGURE 3.5 – Fits to the Lα profile of GD 190. Four different column densities of hydrogen are used. The continuous lines represent photospheric hydrogen abundances of log (H/He) = $-4.0(-0.5) - 6.5$ from the outside in.

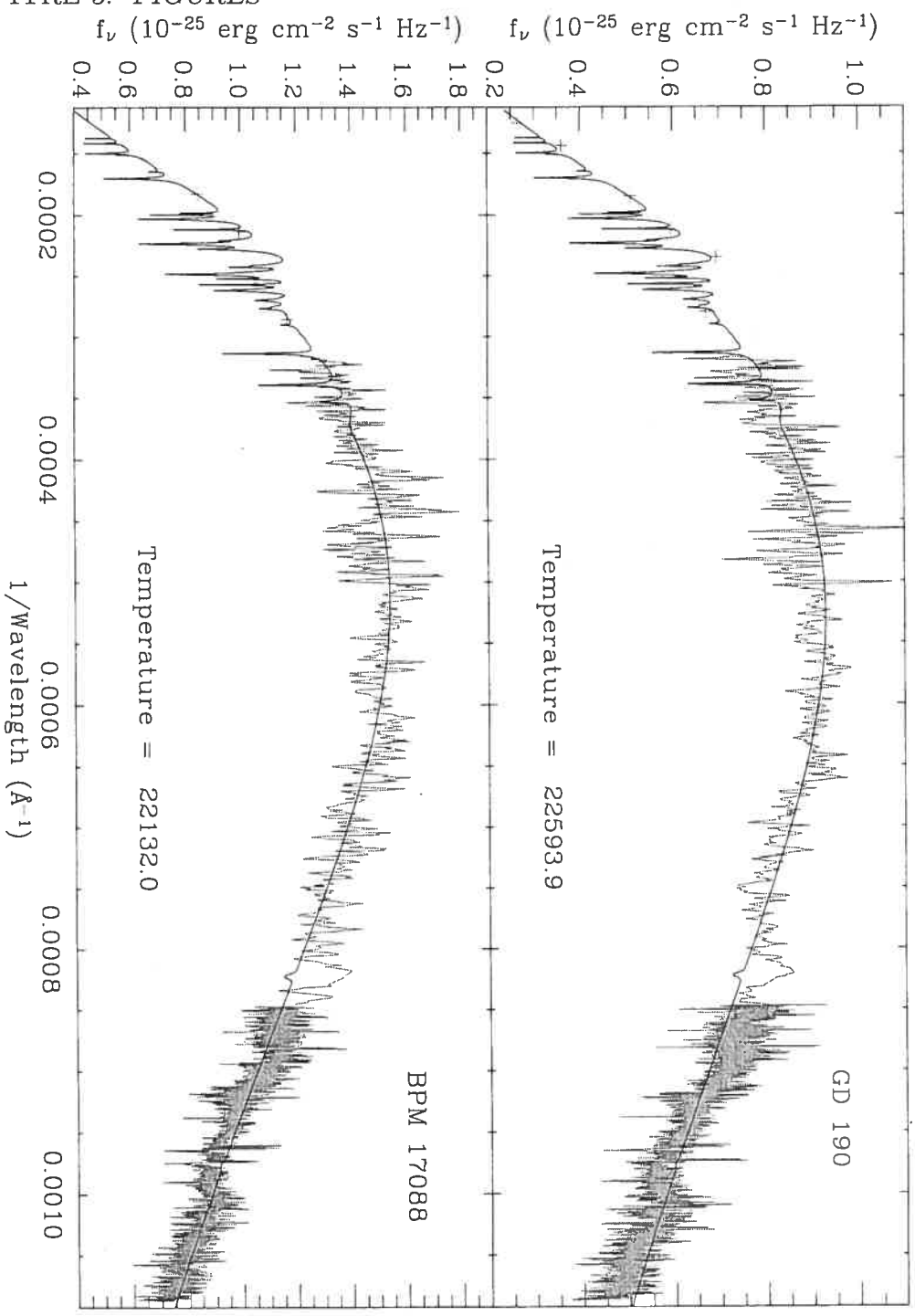

FIGURE 3.6 – Optimal fits to the energy distribution of GD 190 (top panel) and BPM 17088 (bottom panel). In both cases, archival IUE data are combined with existing optical photometry and with FUSE data. Small amounts of interstellar reddening are allowed for in the fits (see text).

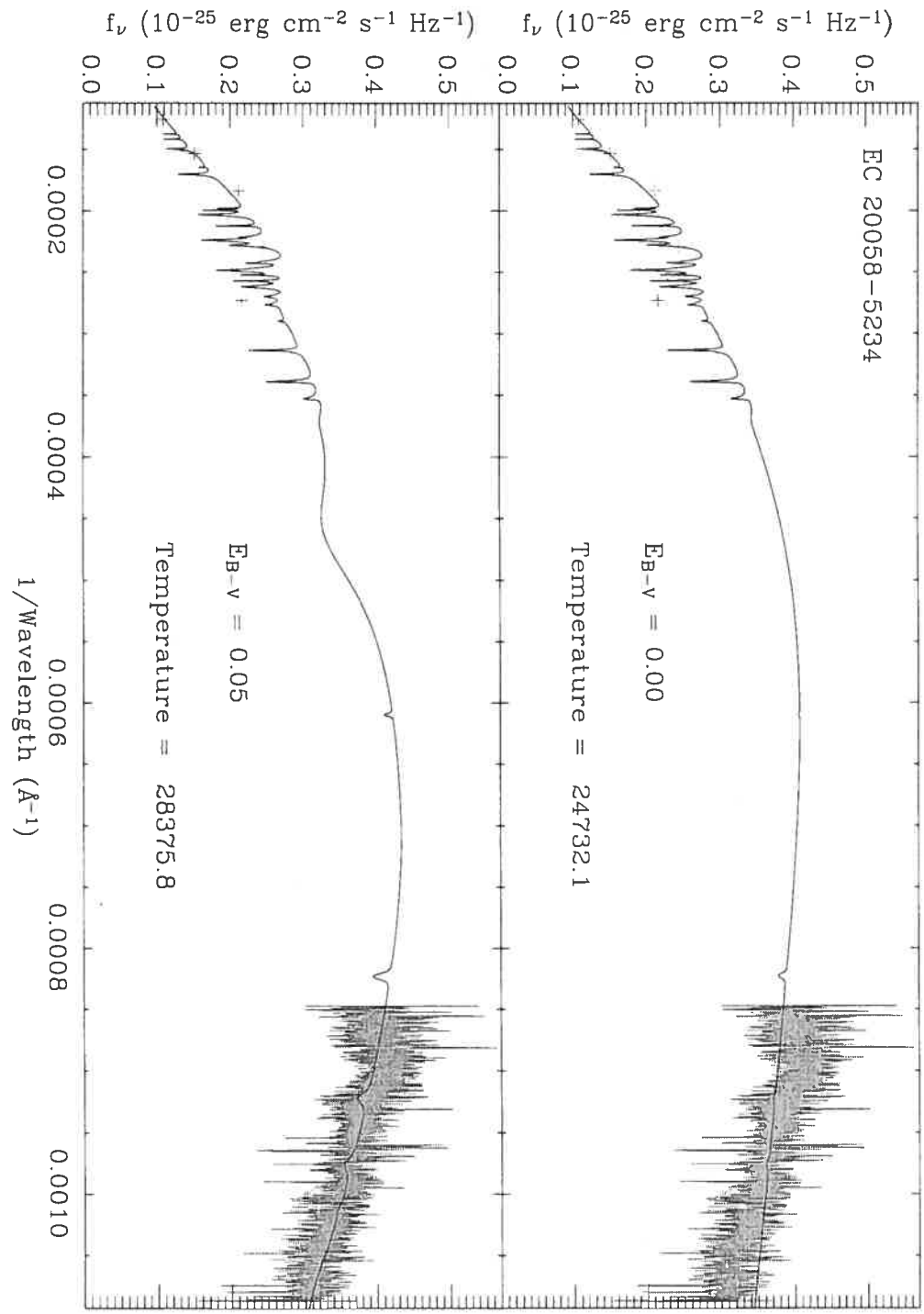

FIGURE 3.7 – Fit to the energy distribution of EC 20058−5234. No archival IUE data exist, and only optical photometry (UBVRI) and FUSE data are available. Attempts to match the data on the basis of no reddening on the line of sight yield an unsatisfactory fit (top pannel). The inclusion of small amounts of reddening, $E_{B-V} = 0.05$, suggests a higher effective temperature and yields a more satisfactory fit to the FUSE data (bottom panel).

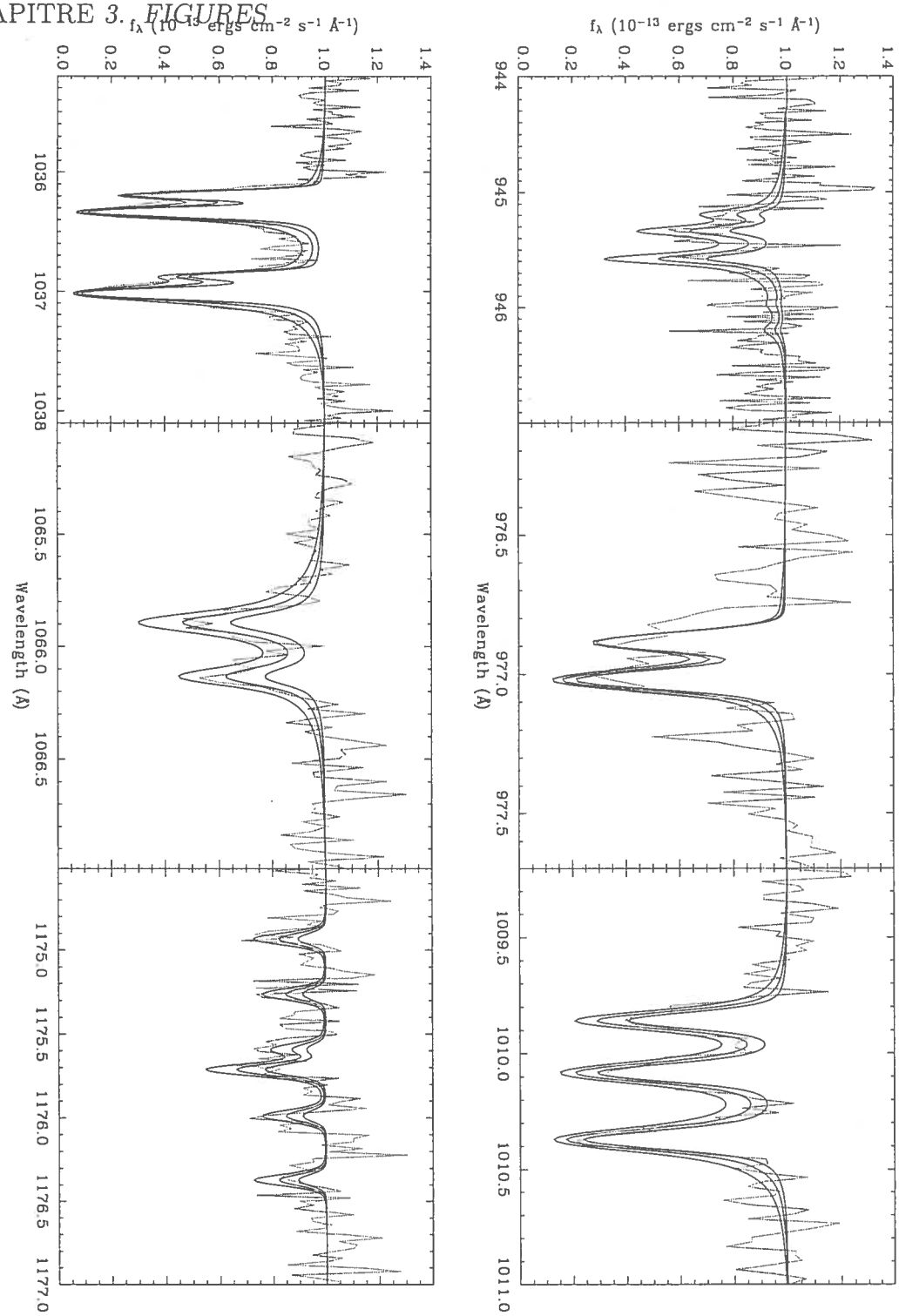

FIGURE 3.8 – Fits to the six carbon features detected in the FUSE spectrum of GD 190. The synthetic spectra are for carbon abundances of log (C/He) of −5.2, −5.5 and −5.8, from bottom to top.

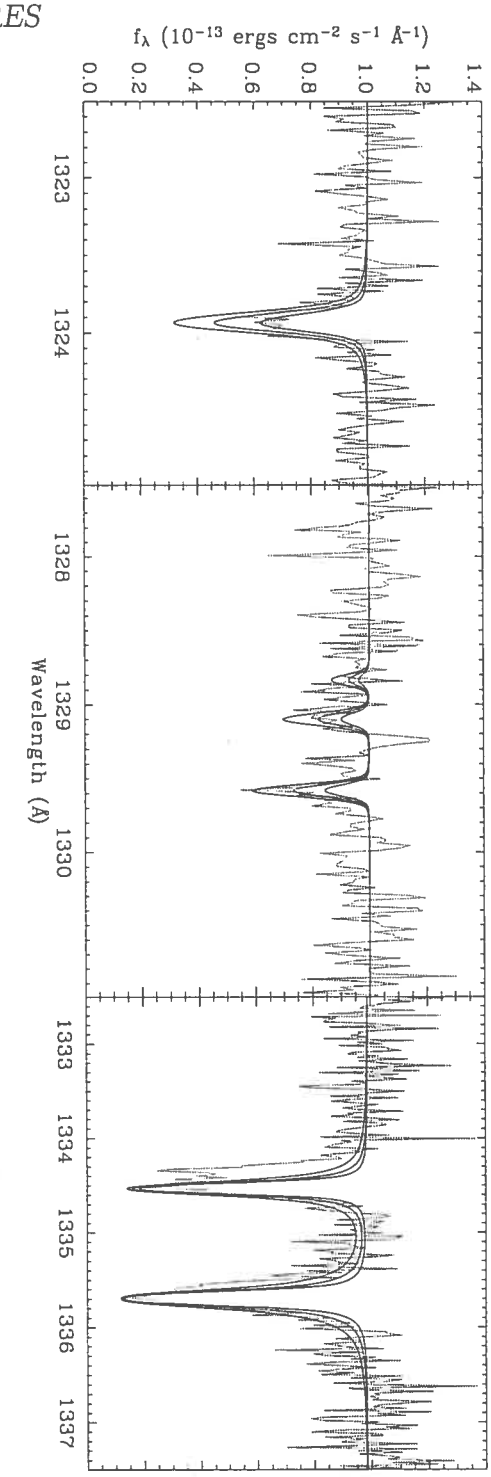

FIGURE 3.9 – Fits to the three carbon features detected in GD 190 by Provencal et al. (2000) in the HST data. The synthetic spectra are for carbon abundances of log (C/He) of -5.2, -5.5 and -5.8, from bottom to top.

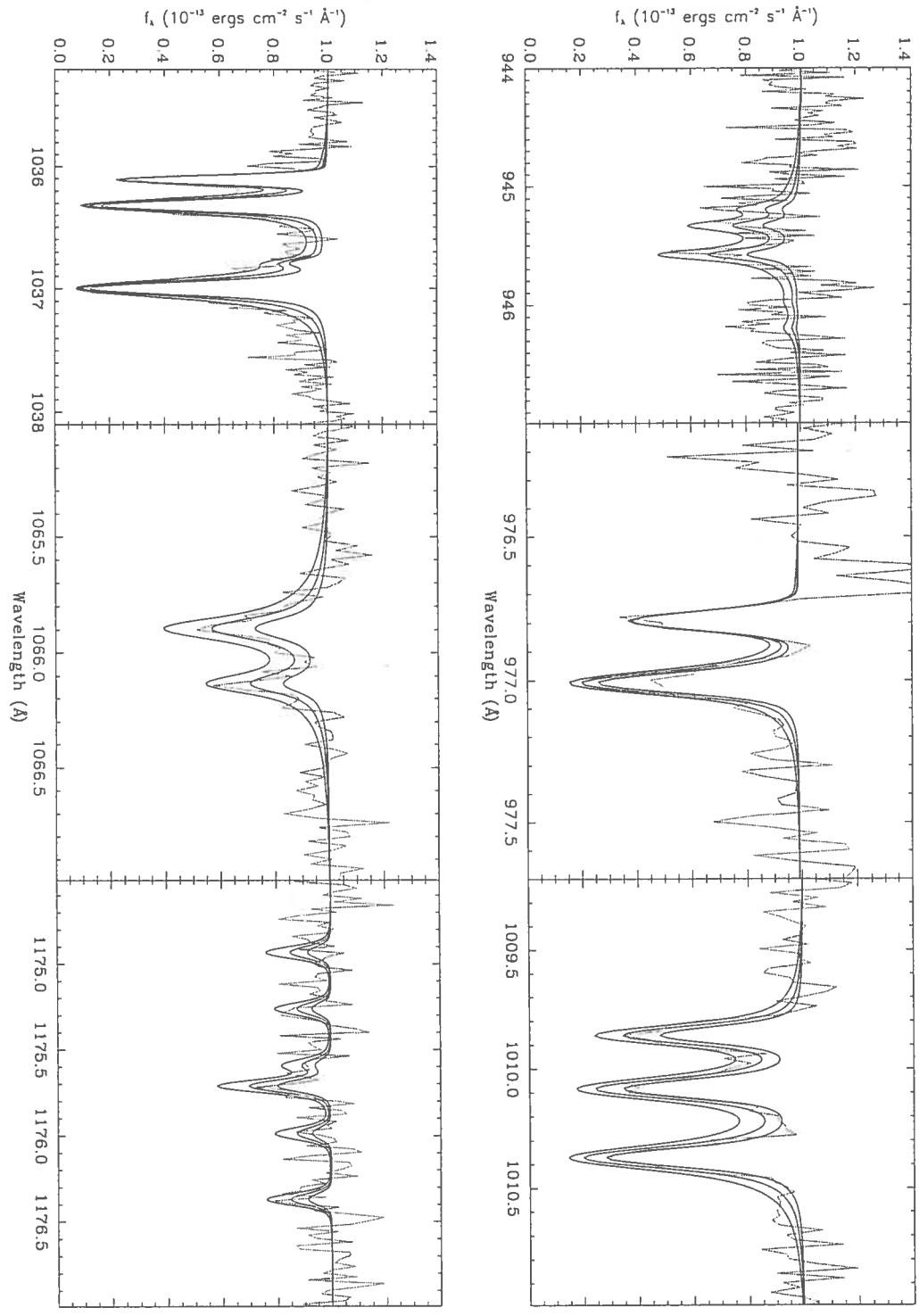

FIGURE 3.10 – Same as Figure 8, but for BPM 17088. The synthetic spectra are for carbon abundances of log (C/He) of −5.2, −5.5 and −5.8, from bottom to top.

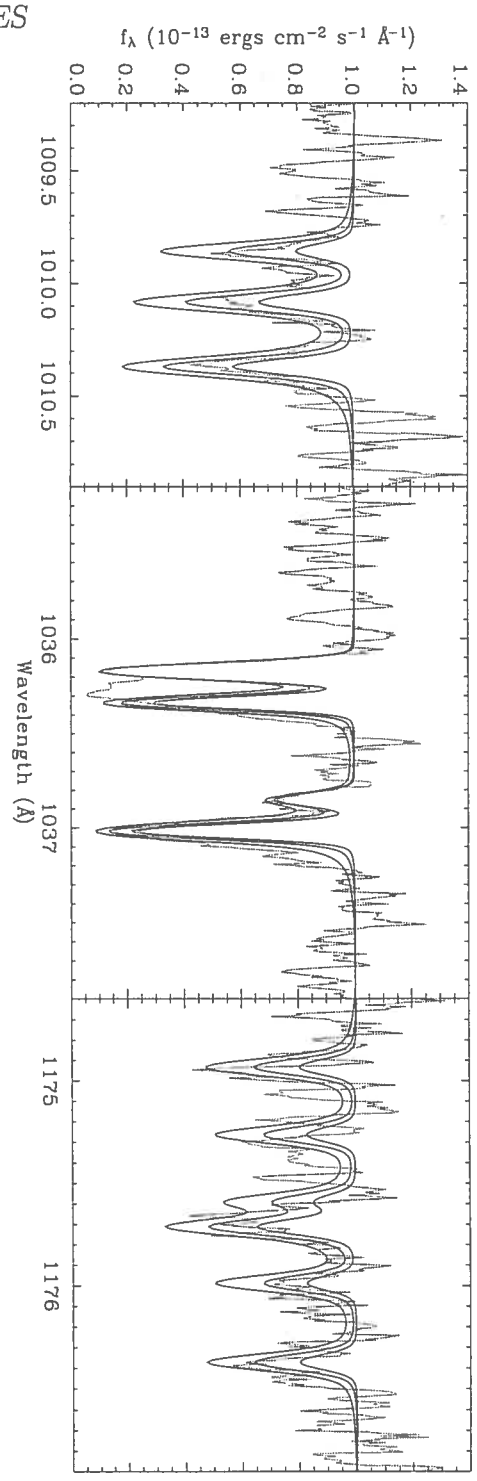

FIGURE 3.11 – Fits to the three carbon features detected in the FUSE spectrum of EC 20058−5234. The synthetic spectra are for carbon abundances of log (C/He) of −5.5, −6.0, and −6.5, from bottom to top.

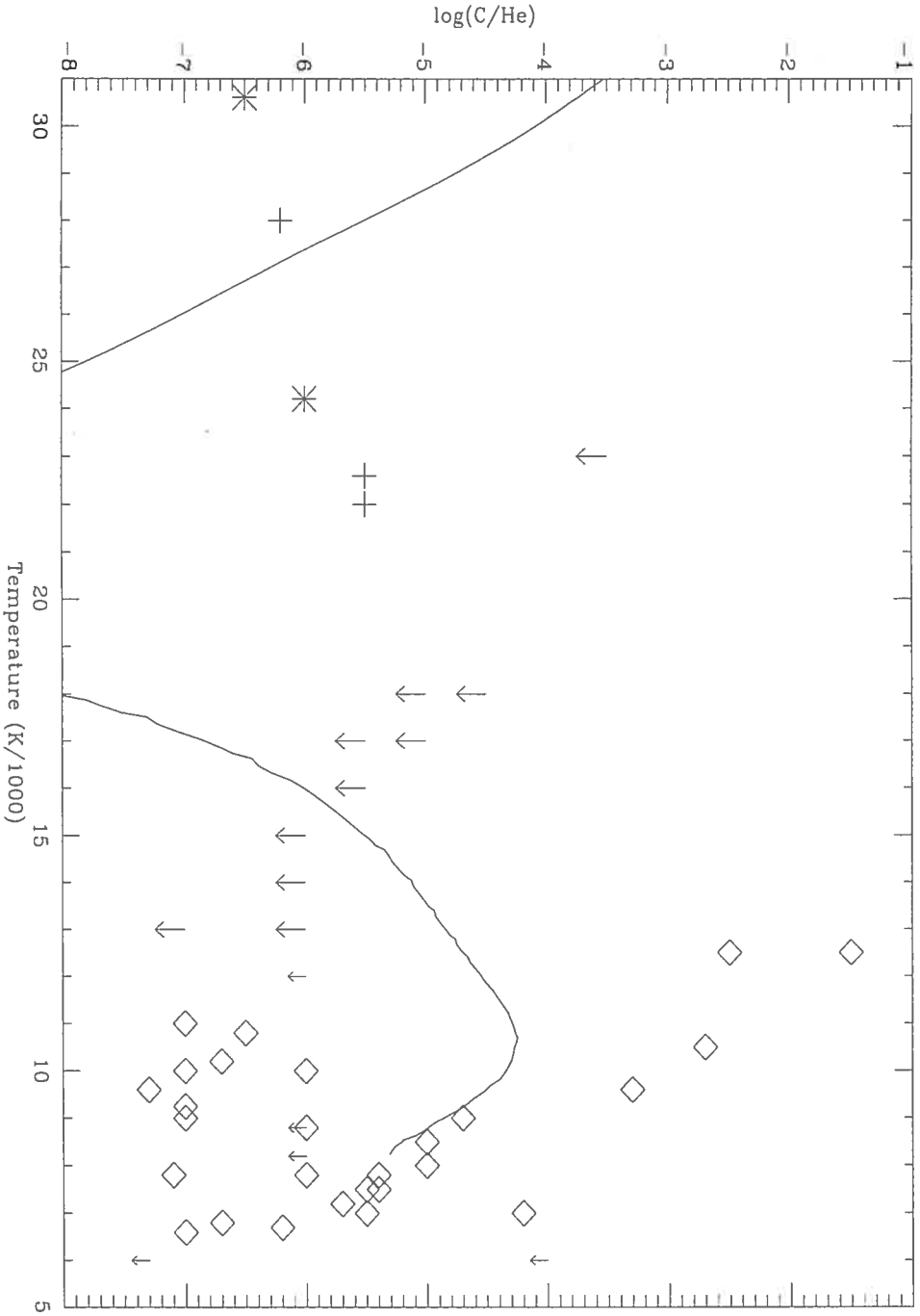

FIGURE 3.12 – Pattern of observed carbon abundances in DB and DQ stars. At the hot end, we have included as crosses the measurements of this paper together with the reanalysis of the GHRS data of Dufour et al. (2004) (stars). The upper limits in DB stars of Wegner & Nelan (1987), as reanalyzed by us, are shown as large arrows. At cooler temperatures, the optical and IUE measurements and upper limits are shown as diamonds and small arrows. The solid line is the expected time-dependent photospheric carbon abundance in an illustrative $0.6\,M_{\odot}$ DB model caracterized by a mass loss rate of the order of $\sim 10^{-13}\,M_{\odot}\,\mathrm{yr}^{-1}$ (see text).

Chapitre 4

Conclusion

Cette étude spectroscopique dans l'ultraviolet lointain de naines blanches de type DB a permis la détermination de l'abondance photosphérique de carbone dans trois étoiles. L'abondance déterminée dans GD 190, log C/He = -5.5, est en bon accord avec la valeur déterminée précédemment à partir du spectre GHRS de cet objet. Celles déterminées dans BPM 17088 et dans EC 20058-5234, soit, respectivement log C/He = -5.5 et log C/He = -6.2, constituent de nouvelles valeurs. L'échantillon d'étoiles de type DB pour lesquelles des mesures du rappport C/He existent inclut maintenant cinq objets. Ces mesures permettent de confirmer que la présence de cet élément ne représente pas un phénomène marginal, mais plutôt un effet systématique devant découler d'une combinaison de processus physiques. Dans ce contexte, la similitude frappante entre GD 190 et BPM 17088, deux étoiles ayant pratiquement la même température effective et présentant la même abondance de carbone, est particulièrement intrigante.

Cette étude, qui porte sur un nombre restreint d'objets, mais qui s'appuie sur une panoplie de données de sources différentes, nous permet d'obtenir, de façon générale, une certaine cohérence dans nos résultats. En particulier, en ce qui concerne la redétermination de la température de GD 190, l'étude des spectres visibles obtenus au Steward Observatory et au Kitt Peak National Observatory est en excellent accord avec celle des spectres

UVES obtenus à l'ESO. Pour la distribution d'énergie, les données photométriques IUE et FUSE se combinent parfaitement et leur modélisation suggère une température très cohérente avec l'analyse des spectres visibles. Les contraintes imposées par les raies de carbone issues de trois états d'ionisation différents sont également cohérentes avec une température de 22 000 K pour GD 190, bien que la sensibilité des raies à la température effective reste relativement faible. Cette méthode n'est donc pas très contraignante.

En plus de l'analyse des spectres dans l'ultraviolet lointain de ces trois objets, nous avons complété la réanalyse des spectres IUE recalibrés disponibles pour la quinzaine d'étoiles incluses dans l'étude de Wegner et Nelan (1987). Ces spectres permettent la détermination d'une limite supérieure à l'abondance de carbone. Pour les DB plus froides, cette limite est fortement contrainte par l'existence de fortes raies de C I dans cette région spectrale, raies qui ne sont toutefois pas observées. La température associée à ces objets, qui n'a pas été remise en question ici, reste cependant beaucoup plus incertaine que celles associées aux trois étoiles à notre programme.

En adoptant la même philosophie, il est également possible de déterminer des limites supérieures à l'abondance de d'autres éléments à partir des spectres FUSE. Des limites relativement contraignantes ont ainsi été déterminées pour le silicium, le fer et le magnésium dans nos trois objets.

L'existence de la raie Lβ dans la région spectrale couverte par FUSE, raie qui n'est pas observée, nous permet également de déterminer une limite supérieure à l'abondance d'hydrogène dans ces objets: log H/He $\leq$ -5.0 pour GD 190 ainsi que pour BPM 17088 et $\leq$ -4.5 pour EC 20058−5234. L'abondance de cet élément ayant un impact important sur la détermination de la température, nous permet de conclure à une température, qui reste incertaine, aux environs de 28 000 K pour EC 20058-5234.

Un résumé de la situation sur l'abondance de carbone pour les étoiles non-DA est présenté sur la figure 2.12 de l'article. Afin d'expliquer cette distribution, incohérente avec la théorie de l'évolution spectrale et son modèle de dragage du carbone, nous

suggérons la présence d'un vent stellaire dans les couches externes des étoiles de type DB. Une perte de masse de l'ordre de $\sim 10^{-13}\ M_{\odot}\ \mathrm{yr}^{-1}$ est suggérée pour ces objets, taux qui n'est pas incohérent avec les valeurs discutées dans la littérature. La présence de ce vent permettrait de ralentir la sédimentation du carbone, qui est présent en abondance dans les progéniteurs des étoiles de type DB, les étoiles de type PG 1159.

Le seul bémol que l'on puisse, à ce stade, apporter à ce scénario est qu'il ne semble pas rendre compte de la tendance observée pour les cinq étoiles de type DB dont l'abondance à été déterminée: l'évidence très préliminaire suggère que les abondances de carbone semblent légèrement à la hausse, ou constantes, au fur et à mesure que l'étoile se refroidit entre 30 000 K et 20 000 K. L'unique modèle de vent considéré suggère, lui, l'existence d'un minimum dans l'abondance de carbone entre 25 000 K et 18 000 K. La situation devrait se clarifier considérablement avec l'observation d'autres étoiles DB en-deça de 20 000 K, prévues dans le cadre du programme d'observation actuellement en cours, et avec une exploration de l'espace des paramètres pour les modèles de vent stellaires.

Annexe A

UVES

Cette section est conçue afin d'expliciter la méthode de réduction utilisée pour réduire des données du spectrographe échelle UVES. Elle explique les rudiments de l'utilisation du pipeline de réduction de données, fourni par l'ESO. Le pipeline est basé sur MIDAS.

L'ESO et le VLT

L'ESO (European Southern Observatory) est une organisation intergouvernementale Européenne de recherche en astronomie. L'ESO opère le VLT (Very Large Telescope) qui consiste en quatre télescopes de 8 mètres pouvant fonctionner de façon indépendante ou combinée. En mode combiné, il constitue le plus grand télescope au monde à observer le domaine visible. Le VLT fait partie de l'observatoire de Cerro Paranal dans le désert de l'Atacama, au nord du Chili.

UVES

Le spectrographe UVES (UV-Visual Echelle Spectrograph) est installé au télescope Kueyen. Il s'agit d'un spectrographe échelle à deux bras de dispersion, un bleu (3000 à

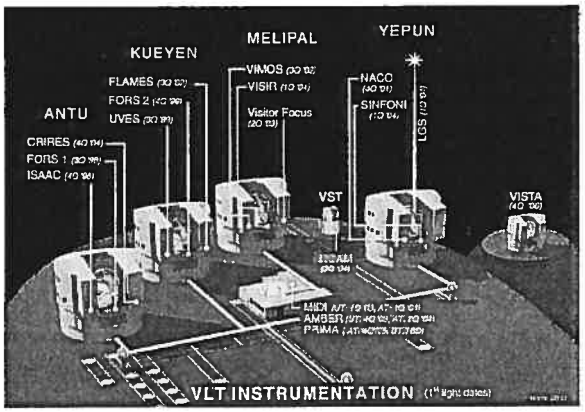

FIGURE A.1 – Schéma du VLT.

5000 Å) et un rouge (4200 à 11000 Å) caractérisés par une résolution spectrale $\lambda/\Delta\lambda$ allant de 110 000 à 18 500 selon le choix de la fente. Le bras bleu est muni d'un détecteur CCD de 2K x 4K pixels ayant chacun une dimension 15μm. Le détecteur du bras rouge est une mosaïque de deux CCD semblables; le spectre rouge est donc séparé en deux sections.

Les archives du VLT

Les données présentes dans les archives de l'ESO/ST-ECF (Space Telescope - European Coordinating Facility) Science Archive Facility sont accessibles de leur site web.[1] Elles sont actuellement disponibles à tous les membres de l'ESO, après une période d'exclusivité d'un an à l'observateur. L'ESO prevoit rendre ses archives disponibles à la communauté internationnale lorsque le maintien des données sera fait de façon uniforme et de bonne qualité.[2]

Les archives fournissent pour un objet donné les différentes expositions et leurs fichiers de calibration bruts respectifs, ainsi que les fichiers de calibration traités par le pipeline. Ces derniers peuvent être utilisés afin d'obtenir directement, à l'aide du

[1] http://archive.eso.org
[2] http://archive.eso.org/Archive_Access_Policy.html

pipeline, le spectre calibré d'un objet. Les fichiers de calibration optimaux associés à une exposition pour une étoile donnée peuvent être identifié à partir des archives en cliquant sur "filelist". En cas de problème avec cette réduction semi-automatisée, le pipeline offre tous les outils nécessaires afin de refaire la calibration des données brutes étape par étape. Toutes les informations à cette fin sont explicitées dans les manuels fournis par l'ESO.[3] Il sera uniquement question ici de la méthode de réduction semi-automatisé.

Réduction des données

La réduction des données est faite de façon semi-automatisée avec le pipeline dévelopé par l'ESO. Ce dernier fontionne sous le système ESO-MIDAS (ESO - Munich Image Data Analysis System).

Le système ESO-MIDAS offre des outils généraux pour le traitement d'images et la réduction de données avec l'accent sur les applications astrophysiques. ESO-MIDAS est distribué gratuitement sous la GNU General Public License.

Le pipeline fonctionne dans le contexte UVES de ESO-MIDAS, un contexte dévelopé spécifiquement pour la réduction de données du spectrographe UVES.

La façon la plus simple de réduire les données est d'utiliser les blocs de réduction (reduction block). Ces derniers sont de simples fichiers ascii où l'on doit spécifier toutes les informations nécessaires à une procédure (recipe) pour réduire les données.

Les procédures nécessaires à la réduction complète des données brutes sont les suivantes:

- Uves_cal_mkmaster: Créer un fichier maître à partir d'une série de fichiers bruts(Bias, Dark, Flat)
- uves_cal_predict: Trouve une première approximation de la calibration en longueur

[3] http://www.eso.org/projects/dfs/dfs-shared/doc/rep/dfs-doc-repository-19500.htm#MAN

d'onde à partir de l'observation à fente courte d'une lampe ThAr.

- uves_cal_orderpos: Trouve la position centrale de chacun des ordres à partir d'un flat.
- uves_cal_wavecal: Trouve la dispersion en longueur d'onde finale, à partir de l'observation à longue fente d'une lampe ThAr.
- **uves_cal_obscired: Fait la réduction d'une exposition à partir des fichiers de calibration créés par les étapes précédentes de la réduction.**

Les fichiers de calibration étant normalement fournis dans les archives, il suffit d'effectuer la dernière étape de la réduction (i.e. uves_cal_obscired).

Étapes de la réduction des données

La réduction des données se résume finalement en trois étapes:

1 -Création des blocs de réduction:

Créer les blocs de réduction appropriés à la procédure uves_cal_obscired pour les 2 sections du spectre i.e. bleu et rouge (ex: uves_cal_obscired_b.rb et uves_cal_obscired_r.rb). Les informations que doivent contenir ces fichiers sont les suivantes:

- Le nom de la prodédure
- Le nom de l'instrument
- Le nom du répertoire où se retrouveront les fichiers produits par la procédure
- Le nom du répertoire et du fichier de l'exposition à réduire et le mot clé représentant le fichier
- Le nom du répertoire et des fichiers de calibration et leur mot clé associé

Exemple pour uves_cal_obscired_b.rb:

```
recipe:  uves_obs_scired

instrument: uves
```

```
/home/nicolas/donnees/vlt/bpm/results/r.b.UVES.2003-05-21

{
/home/nicolas/donnees/vlt/bpm/UVES.2001-10-30T05:41:48.526.fits SCIENCE_BLUE
}
{
/home/nicolas/donnees/vlt/bpm/cal/M.UVES.2001-11-16T10:22:09.499.tfits DRS_SETUP_BLUE
/home/nicolas/donnees/vlt/bpm/cal/M.UVES.2001-11-16T10:24:06.729.tfits ORDER_TABLE_BLUE
/home/nicolas/donnees/vlt/bpm/cal/M.UVES.2001-11-16T10:21:47.893.tfits BACKGR_TABLE_BLUE
/home/nicolas/donnees/vlt/bpm/cal/M.UVES.2001-11-16T10:22:49.121.tfits LINE_TABLE_BLUE1
/home/nicolas/donnees/vlt/bpm/cal/M.UVES.2001-11-16T10:23:16.103.tfits LINE_TABLE_BLUE2
/home/nicolas/donnees/vlt/bpm/cal/M.UVES.2001-11-16T10:23:45.744.tfits LINE_TABLE_BLUE3
/home/nicolas/donnees/vlt/bpm/cal/M.UVES.2001-11-16T09:28:46.298.fits MASTER_BIAS_BLUE
/home/nicolas/donnees/vlt/bpm/cal/M.UVES.2001-11-16T10:24:29.003.fits MASTER_FLAT_BLUE
}
```

Pour la section rouge du spectre, la réduction de ses deux sous sections (Upper et Lower) se fait en simultané. Exemple pour uves_cal_obscired_r.rb:

```
recipe:  uves_obs_scired

instrument: uves

/home/nicolas/donnees/vlt/bpm/results/r.red.UVES.2003-05-30

{
/home/nicolas/donnees/vlt/bpm/UVES.2001-10-30T05:43:59.596.fits SCIENCE_RED
}
{
/home/nicolas/donnees/vlt/bpm/cal/M.UVES.2001-11-16T10:22:14.414.tfits DRS_SETUP_REDL
/home/nicolas/donnees/vlt/bpm/cal/M.UVES.2001-11-16T10:24:11.156.tfits ORDER_TABLE_REDL
/home/nicolas/donnees/vlt/bpm/cal/M.UVES.2001-11-16T10:21:54.369.tfits BACKGR_TABLE_REDL
/home/nicolas/donnees/vlt/bpm/cal/M.UVES.2001-11-16T10:22:53.074.tfits LINE_TABLE_REDL1
```

```
/home/nicolas/donnees/vlt/bpm/cal/M.UVES.2001-11-16T10:23:21.437.tfits LINE_TABLE_REDL2
/home/nicolas/donnees/vlt/bpm/cal/M.UVES.2001-11-16T10:23:49.732.tfits LINE_TABLE_REDL3
/home/nicolas/donnees/vlt/bpm/cal/M.UVES.2001-11-16T09:29:35.115.fits MASTER_BIAS_REDL
/home/nicolas/donnees/vlt/bpm/cal/M.UVES.2001-11-16T10:24:34.280.fits MASTER_FLAT_REDL

/home/nicolas/donnees/vlt/bpm/cal/M.UVES.2001-11-16T10:22:23.368.tfits DRS_SETUP_REDU
/home/nicolas/donnees/vlt/bpm/cal/M.UVES.2001-11-16T10:24:15.217.tfits ORDER_TABLE_REDU
/home/nicolas/donnees/vlt/bpm/cal/M.UVES.2001-11-16T10:21:58.828.tfits BACKGR_TABLE_REDU
/home/nicolas/donnees/vlt/bpm/cal/M.UVES.2001-11-16T10:23:02.061.tfits LINE_TABLE_REDU1
/home/nicolas/donnees/vlt/bpm/cal/M.UVES.2001-11-16T10:23:31.718.tfits LINE_TABLE_REDU2
/home/nicolas/donnees/vlt/bpm/cal/M.UVES.2001-11-16T10:23:58.437.tfits LINE_TABLE_REDU3
/home/nicolas/donnees/vlt/bpm/cal/M.UVES.2001-11-16T09:30:57.741.fits MASTER_BIAS_REDU
/home/nicolas/donnees/vlt/bpm/cal/M.UVES.2001-11-16T10:25:36.240.fits MASTER_FLAT_REDU
}
```

2 -Exécution des blocs de réduction dans MIDAS:

Il faut ensuite initialiser MIDAS à l'aide du programme pipe.prg. Ce programme lance le contexte UVES de MIDAS et permet l'utilisation des blocs de réduction. On peut le faire de la façon suivante:

```
xhost +
rlogin titan
setenv DISPLAY ${REMOTEHOST}:0
## Aller dans le repertoire du pipeline contenant le fichier pipe.prg
cd uves_2.0.0/fluves/ex/rb
\#\# Ouvrir MIDAS
inmidas -P -j "@@ pipe.prg"
```

Ensuite, il suffit d'exécuter les blocs de réduction de la manière suivante:

```
execute/rb /home/.../uves_obs_scired_b.rb
execute/rb /home/.../uves_obs_scired_r.rb
```

La procédure produit plusieurs fichiers numerotés de 0000 à 0010 pour le spectre bleu et de 0000 à 0021 pour les spectres rouges. Les spectres calibrés finals sont les fichiers 0000(bleu), 0000(rouge) et 0011(rouge).

3 -Calibration en flux des spectres réduits dans IDL:

Les spectres produits ne sont cependant pas calibrés en flux. Cette étape finale de la réduction est effectuée à l'aide d'un programme idl maison, qui exécute la recette indiqué par l'ESO.[4] Ce dernier va lire dans l'entête(header) du fichier .fits du spectre réduit les mots-clés(keywords) suivants:

- EXPTIME: Le temps d'exposition
- CONAD: Facteur de conversion d'électrons à photons
- BINX: Sommation de pixels
- AIRMASS: La masse d'air au moment de l'observation

Ce qui permet de faire certaines corrections au spectre. La calibration en flux ne se fait cependant pas de façon traditionnelle avec l'observation d'une étoile standard. L'ESO fournit des fichiers (MASTER_RESPONSE)[5] pour chacune des configurations de l'instrument (i.e. longueur d'onde centrale des spectres) et pour une période de temps donnée. Ces fichiers décrivent la sensibilité des détecteurs basée sur l'observation de plusieurs étoiles standard. Le programme fait simplement la multiplication du spectre calibré et corrigé par le fichier MASTER_RESPONSE approprié; le spectre résultant est calibré en flux ($\mathbf{10^{-16}\ erg/s/cm^2/\text{Å}}$).

Voici un exemple de ce programme pour calibrer la section bleue du spectre de BPM 17088 *fluxerbpm_vlt_b.pro* (évidemment certains paramètres doivent être ajustés en fonction de l'objet et de la région spectrale à calibrer):

```
pro fluxergd_vlt_b,saveplot=saveplot

; ------- Parametres a modifier -----------------------------
```

[4] http://www.eso.org/observing/dfo/quality/UVES/qc/response.html
[5] http://www.eso.org/observing/dfo/quality/UVES/qc/std_qc1.html#response

```
; Spectre a calibrer
spectre_filename ='/home/nicolas/donnees/vlt/bpm/results/r.b.UVES.2003-05-21_0000.fits'
; Nom du fichier ou sauver le graphique
ps_filename = '/home/nicolas/.../bleue_fluxe.ps'
; Fichier MASTER_RESPONSE
MR_filename = '/home/nicolas/.../UV_MRSP_020801_BLUE390.tfits'
; Localiser le fichier contenant l'information sur la masse d'air (fournit avec le pipeline)
atm_filename = '/home/nicolas/.../fluves/calib/atmoexan.fits'
; Nom du fichier ou sauver le spectre calibre en flux
asc_filename = '/home/nicolas/.../bpm_vlt_b.dat'
; Lire dans le header du spectre le keyword: HIERARCH ESO DET OUT1 CONAD
conad = 0.6
; Lire dans le header du spectre le keyword: HIERARCH ESO DET WIN1 BINX
binx = 2.
; ------------------------------------------------------------

if keyword_set(saveplot) then begin
 old_dev=!D.NAME
 set_plot, 'PS'
device, /landscape, FILE=ps_filename
endif

!p.multi=[0,1,1]

; Ouverture du spectre
reduced = readfits(spectre_filename,h)

; Creation du vecteur de longueur d'onde
sizetemp = size(reduced)
size= sizetemp(1)
pas = sxpar(h,'CDELT1')
w0 = sxpar(h,'CRVAL1')
```

```
w = findgen(size)*pas+w0

; Lecture des parametres
exptime = sxpar(h,'EXPTIME')
print, 'Temps d exposition=', exptime
print,'Conad(verifier) =',conad
print, 'Binx(verifier) =',binx
airmass = sxpar(h,'AIRMASS')
wlen1 = sxpar(h,'WLEN1')
print,'Grating central wavelength =',wlen1

; Normalisation du spectre
norm = reduced/exptime
norm_conad = norm*conad
norm_bin = norm_conad/binx

; Extinctions
atm = readfits(atm_filename,htab,/EXTEN)
watm = tbget(htab, atm, 1)
exatm = tbget(htab, atm, 2)
linterp, watm,exatm,w,extinction
norm_exti = norm_bin*10^(0.4*extinction*airmass)

; ---- Courbe de reponse
mast_res = readfits(MR_filename,hmas,/EXTEN)
wmas = tbget(hmas, mast_res, 1)
mas = tbget(hmas, mast_res, 2)
linterp, wmas,mas,w,master_response
; ----

fluxed_science_m = norm_exti*master_response
```

```
plot,w,fluxed_science_m, xstyle =1, xrange=[3250,4550],yrange = [0,200],
& ytitle = '10e-16 erg/s/cm**2/A', xtitle='A', title='Spectre bleue fluxe; Master_cal'

; Sauvegarde du spectre blue
f=fluxed_science_m

; Enlever les zeros
range=where(f ne 0.)
w=w(range)
f=f(range)

;SAVE, FILENAME = '/home/nicolas/.../vlt_blue.sav',w,f
asc_write,asc_filename,w,f

if keyword_set(saveplot) then begin
 device, /close
 set_plot, old_dev
endif

end
```

Bibliographie

Beauchamp, A., Wesemael, F., Bergeron, P., Liebert, J., & Saffer, R.A. 1996, in Hydrogen-Deficient Stars, eds. C.S. Jeffery & U. Heber, (San Francisco; A.S.P.), p. 295

Beauchamp, A., Wesemael, F., Bergeron, P., Fontaine, G., Saffer, R.A., Liebert, J. & Brassard, P. 1999, ApJ, 516, 887

Beers, T.C., Preston, G.W., Shectman, S.A., Doinidis, S.P., & Griffin, K.E. 1992, AJ, 103, 267

Bergeron, P., Wesemael, F., & Beauchamp, A. 1995, PASP, 107, 1047

Bessell, M.S. 1990, PASP, 102, 1181

Bessell, M.S. & Wickramasinghe, D.T. 1978, MNRAS, 182, 275

Brassard, P. & Fontaine, G. 2002, ApJL, 581, L33

Brassard, P. & Fontaine, G. 2003, in White Dwarfs, eds. D. de Martino, R. Silvotti, J.-E. Solheim, & R. Kalytis, (Dordrecht: Kluwer), p. 259

Brassard, P. & Fontaine, G. 2004, private communication

Burstein, D. & Heiles, C. 1982, AJ, 87, 1165

Chayer, P., Fontaine, G. & Wesemael, F. 1995, ApJS, 99, 189

Dehner, B.T. & Kawaler, S. 1995, ApJL, 445, L141

Dufour, P., Wesemael, F., & Bergeron, P. 2002, ApJ, 575, 1025

Dufour, P., Wesemael, F., & Bergeron, P. 2004, in preparation

Fontaine, G., Villeneuve, B., Wesemael, F., & Wegner, G. 1984, ApJ, 277, L61

Fontaine, G. & Wesemael, F. 1987, IAU Colloq. 95: Second Conference on Faint Blue Stars, 319

Fontaine, G. & Wesemael, F. 1991, IAU Symp. 145: Evolution of Stars: the Photospheric Abundance Connection, 145, 421

Friedrich, S., Koester, D., Christlieb, N., Reimers, D. & Wisotzki, L. 2000, AA, 363, 1040

Friedrich, S., Jordan, S., & Koester, D. 2003, in White Dwarfs, eds. D. de Martino, R. Silvotti, J.E. Solheim & R. Kalytis (Dordrecht: Kluwer), p. 203

Greenstein, J.L. 1984, ApJ, 276, 602

Heber, U., Hunger, K., Jonas, G. & Kudritzki, R.P. 1984, AA, 130, 119

Holberg, J.B., Barstow, M.A. & Burleigh, M.R. 2003, ApJS, 147, 145

Hubeny, I. & Lanz, T. 1995, ApJ, 439, 875

Hunter, C. 2001, M.Sc. thesis, Université de Montréal

Koen, C., O'Donoghue, D., Stobie, R.S., Kilkenny, D., & Ashley, R. 1995, MNRAS, 277, 913

Koester, D., Schulz, H., & Wegner, G. 1981, AA, 102, 331

Koester, D. & Weidemann, V. 1982, Å, 108, 406

Koester, D., Weidemann, V., & Zeidler-K.T. 1982, Å, 116, 147

Koester, D. et al. 2001, AA, 378, 556

Liebert, J., Beaver, E.A., Robertson, J.W., & Strittmatter, P.A. 1977, ApJL, 204, L119

Liebert, J., Wesemael, F., Hansen, C.J., Fontaine, G., Shipman, H.L., Sion, E.M., Winget, D.E., & Green, R.F. 1986, ApJ, 309, 241

MacDonald, J., Hernanz, M., & José, J. 1998, MNRAS, 296, 523.

Napiwotzki, R. et al. 2001, AN, 322, 411

Oke, J.B., Weidemann, V. & Koester, D. 1984, ApJ, 281, 276

Olson, E.C. 1974, PASP, 86, 80

Pelletier, C., Fontaine, G., Wesemael, F., Michaud, G., & Wegner, G. 1986, ApJ, 307, 242

Provencal, J.L., Shipman, H.L., Thejll, P., Vennes, S., & Bradley, P.A. 1996, ApJ, 466, 1011

Provencal, J.L., Shipman, H.L., Thejll, P., & Vennes, S. 2000, ApJ, 542, 1041

Savage, B.D., Sembach, K.R., Tripp, T.M., & Richter, P. 2002, ApJ, 564, 631

Spitzer, L., Jr. 1978, Physical Processes in the Interstellar Medium (New York: Wiley)

Thejll, P., Vennes, S. & Shipman, H.L. 1991, ApJ, 370, 355

Unglaub, K. & Bues, I. 2000, AA, 359, 1042

Vauclair, G., Vauclair, S., & Greenstein, J.L. 1979, AA, 80, 79

Wegner, G. 1979, MNRAS, 166, 271

Wegner, G. 1979, AJ, 84, 1384

Wegner, G. & Nelan, E.P. 1987, ApJ, 319, 916

Wesemael, F., Greenstein, J. L., Liebert, J., Lamontagne, R., Fontaine, G., Bergeron, P., & Glaspey, J. W. 1993, PASP, 105, 761

Wesemael, F. & Truran, J.W. 1982, ApJ, 260, 807

Winget, D.E., Sullivan, D.J., Metcalfe, T.S., Kawaler, S.D., & Montgomery, M.H. 2004, ApJL, 602, L109

Zuckerman, B., Koester, D., Reid, I.N., & Hünsch, M. 2003, ApJ, 596, 477

Remerciements

Je tiens à remercier tout d'abord François Wesemael pour son immense support durant une bonne partie de mes études universitaires ainsi que pour la réalisation de ce document. Une ode toute particulière à son talent et ses efforts pédagogiques qui ont clairement su stimuler mon intéret pour l'astrophysique.

Hommage à Gilles Fontaine dont la passion pour la science est contagieuse, une véritable source d'inspiration.

Pierre Chayer a également été une personne ressource déterminante pour tout ce qui concernait les spectres FUSE et IDL.

Ce projet a de plus gagné en profondeur grâce à l'apport de Malvina Billères, qui nous a fourni les spectres UVES.

Un très sincère merci à tous.